lost their excess weight by 17 weeks of age (Fig. 1a). This is attributable to the development of overt diabetes due to severe insulin deficiency (Fig. 1b, c). In fact, non-fasted blood glucose levels of *Wfs1*$^{-/-}$ *A*^{y}*/a* mice started to rise significantly from the age of 8 weeks, with all *Wfs1*$^{-/-}$ *A*^{y}*/a* mice developing overt diabetes by 16 weeks of age (Fig. 1b). Ketosis manifested after age 16 weeks (data not shown). In contrast, blood glucose levels of *Wfs1*$^{+/+}$ *A*^{y}*/a* and *Wfs1*$^{-/-}$ *a/a* mice did not differ from those of WT mice. We also examined plasma insulin levels of these mice. At 12 weeks of age, the plasma insulin levels of *Wfs1*$^{+/+}$ *A*^{y}*/a* mice were significantly higher than those of WT littermates, and *Wfs1*$^{-/-}$ *a/a* and *Wfs1*$^{-/-}$ *A*^{y}*/a* mice. Interestingly, *Wfs1*$^{-/-}$ *A*^{y}*/a* mice tended to be more hyperinsulinaemic than *Wfs1*$^{-/-}$ *a/a* and WT at this age, although the differences did not reach statistical significance. However, at 24 weeks of age, plasma insulin levels in *Wfs1*$^{-/-}$ *A*^{y}*/a* mice were markedly decreased (Fig. 1c).

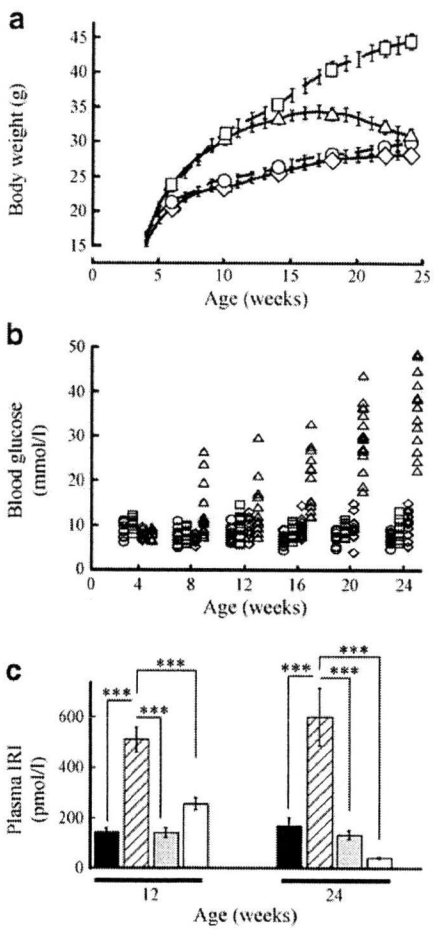

Fig. 1 Weight, blood glucose and insulin levels of *Wfs1*$^{-/-}$ *A*^{y}*/a* and other mice. **a** Weight of *Wfs1*$^{-/-}$ *A*^{y}*/a* (triangles), *Wfs1*$^{+/+}$ *A*^{y}*/a* (squares), *Wfs1*$^{-/-}$ *a/a* (diamonds) and *Wfs1*$^{+/+}$ *a/a* (WT, circles) mice over the course of 24 weeks. Values are the means±SE for n=14–21 mice. **b** Non-fasted blood glucose levels in *Wfs1*$^{-/-}$ *A*^{y}*/a*, *Wfs1*$^{+/+}$ *A*^{y}*/a*, *Wfs1*$^{-/-}$ *a/a* and WT mice; key as above, n=11–16. $p<0.05$ for *Wfs1*$^{-/-}$ *A*^{y}*/a* vs *Wfs1*$^{+/+}$ *A*^{y}*/a*, *Wfs1*$^{-/-}$ *a/a* and WT mice at 8 and 12 weeks; $p<0.001$ for *Wfs1*$^{-/-}$ *A*^{y}*/a* vs *Wfs1*$^{+/+}$ *A*^{y}*/a*, *Wfs1*$^{-/-}$ *a/a* and WT mice at 16, 20 and 24 weeks. **c** Plasma immunoreactive insulin (IRI) levels in *Wfs1*$^{-/-}$ *A*^{y}*/a* (white bars), *Wfs1*$^{+/+}$ *A*^{y}*/a* (hatched bars), *Wfs1*$^{-/-}$ *a/a* (grey bars) and WT (black bars) mice at 12 and 24 weeks of age. Data are presented as the means±SE for n=7–13 mice. ***$p<0.001$

Intraperitoneal glucose tolerance test and ITT were performed at 8 weeks (Fig. 2). *Wfs1*$^{+/+}$ *A*^{y}*/a* mice, as well as *Wfs1*$^{-/-}$ *A*^{y}*/a* mice, were already more insulin-resistant than *Wfs1*$^{+/+}$ *a/a* and *Wfs1*$^{-/-}$ *a/a* mice at this young age (Fig. 2a, d). There was no statistical difference in the ITT curve between *Wfs1*$^{+/+}$ *A*^{y}*/a* and *Wfs1*$^{-/-}$ *A*^{y}*/a* mice. Although glucose tolerance of *Wfs1*$^{+/+}$ *A*^{y}*/a* mice was normal because of compensatory elevated insulin secretion (Fig. 2b, c), this compensation was not found in *Wfs1*$^{-/-}$ *A*^{y}*/a* mice, whose glucose tolerance was impaired (Fig. 2e, f).

A similar, but milder phenotype was observed in the *Wfs1*$^{-/-}$ *a/a* mice with high-fat diet-induced obesity (ESM Fig. 1). The high-fat diet caused obesity with hyperinsulinaemia in WT mice (*Wfs1*$^{+/+}$ *a/a*). However, these mice were normoglycaemic (ESM Fig. 1a). In contrast, a high-fat diet induced hyperglycaemia in *Wfs1*$^{-/-}$ *a/a* mice, although less prominently than in *Wfs1*$^{-/-}$ *A*^{y}*/a* mice (mean non-fasting blood glucose 18.0±2.7 mmol/l, n=6 vs 36.9±2.4 mmol/l, n=14 at 24 weeks of age, $p<0.001$) (ESM Fig. 1b). Non-fasting insulin levels were lower, although not significantly, in high-fat diet-fed *Wfs1*$^{+/+}$ *a/a* than in *Wfs1*$^{+/+}$ *A*^{y}*/a* mice (402.9±87.5 pmol/l, n=9 vs 605.7±114.4, n=7 at age 24 weeks, $p>0.05$) (ESM Fig. 1c).

Acceleration of selective beta cell apoptosis We immunohistochemically investigated the cause of insulin deficiency. In 24-week-old *Wfs1*$^{+/+}$ *A*^{y}*/a* mice, islets were hypertrophic and larger (Fig. 3b, f, j) than in WT (Fig. 3a, e, i) and *Wfs1*$^{-/-}$ *a/a* mice (Fig. 3c, g, k), reflecting responses to the increased insulin demand in *Wfs1*$^{+/+}$ *A*^{y}*/a* mice. In the *Wfs1*$^{-/-}$ *a/a* mice, insulin-positive beta cells were preserved (Fig. 3c, g) and there was no apparent difference from WT controls at this stage, except for a change in islet architecture (aberrant centric migration of alpha cells) (Fig. 3g, [15]). Interestingly and impressively, however, *Wfs1*$^{-/-}$ *A*^{y}*/a* mice had small, irregularly shaped islets, in which insulin-positive beta cells were markedly decreased (Fig. 3d, h).

The results were confirmed by morphometric analysis showing that the insulin-positive area per pancreatic area in *Wfs1*$^{+/+}$ *A*^{y}*/a* mice was increased as compared with that in WT and *Wfs1*$^{-/-}$ *a/a* mice. In *Wfs1*$^{-/-}$ *A*^{y}*/a* mice, the insulin-positive area was markedly reduced (Fig. 4a), as was the pancreatic insulin content (Fig. 4b).

Time courses of beta cell loss in *Wfs1*$^{-/-}$ *A*^{y}*/a* islets are shown in Fig. 3m–o. In *Wfs1*$^{-/-}$ *A*^{y}*/a* mice, insulin-positive beta cells were selectively and severely depleted by

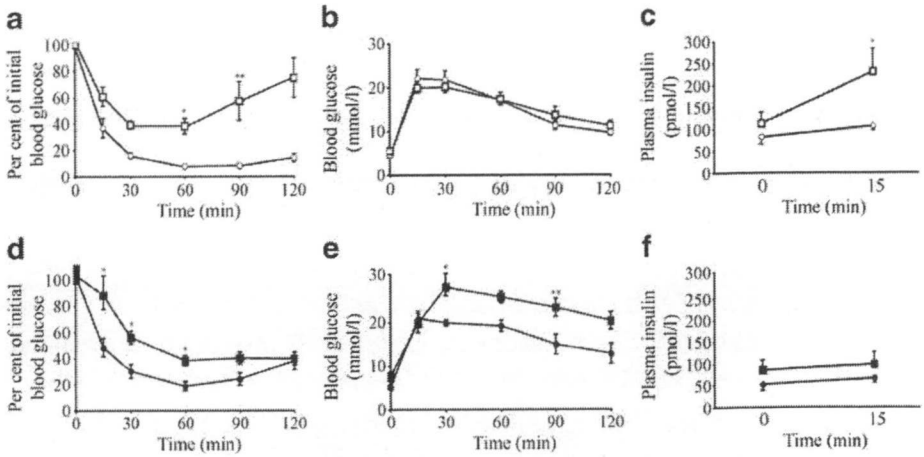

Fig. 2 Insulin tolerance test and ipGTT. ITT (0.75 U/kg) (**a**, **d**) and ipGTT (2 g/kg) (**b**, **c**, **e**, **f**) were performed at 8 weeks of age on *Wfs1*$^{+/+}$ *a/a* (WT) (white circles), *Wfs*$^{+/+}$ *A*^{y}*/a* (white squares), *Wfs1*$^{-/-}$ *a/a* (black circles) and *Wfs1*$^{-/-}$ *A*^{y}*/a* (black squares). Values are means±SEM, n=3–10 per group (ITT) and n=7–10 per group (ipGTT). *p<0.05, **p<0.01 compared with the corresponding *a/a* mice

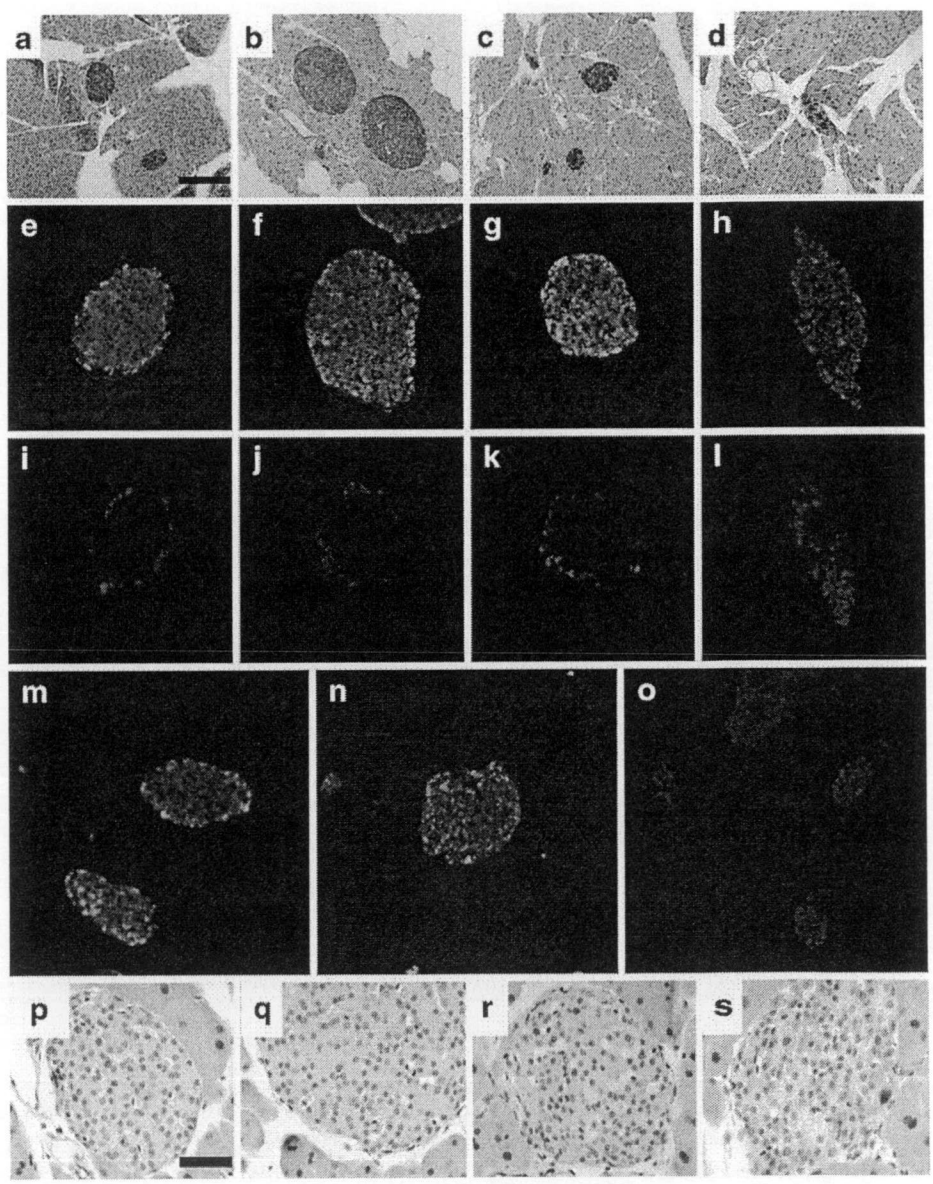

Fig. 3 Selective beta cell loss in islets of *Wfs1*$^{-/-}$ *A*^{y}*/a* mice. **a–l** Pancreatic sections from 24-week-old *Wfs1*$^{+/+}$ *a/a* (WT), *Wfs1*$^{+/+}$ *A*^{y}*/a*, *Wfs1*$^{-/-}$ *a/a* and *Wfs1*$^{-/-}$ *A*^{y}*/a* mice were immunostained for insulin (brown) (**a–d**), scale bar 100 nm. **e–h** Immunofluorescence staining for insulin (green), glucagon (red) and (**i–l**) somatostatin (red). **m–o** Representative time course of beta cell loss in islets from *Wfs1*$^{-/-}$ *A*^{y}*/a* mice. Insulin (green) and glucagon (red) were immunostained. At 8 weeks (**m**), most islets were indistinguishable from those of WT mice. By the 16th week (**n**), normal islet architecture had been destroyed and beta cell numbers were apparently decreased. By week 24 (**o**), few beta cells remained. **p–s** Immunohistochemistry results for pro-apoptotic active caspase-3 in pancreatic sections from WT (**p**), *Wfs1*$^{+/+}$ *A*^{y}*/a* (**q**), *Wfs1*$^{-/-}$ *a/a* (**r**) and *Wfs1*$^{-/-}$ *A*^{y}*/a* mice (**s**). Activated caspase-3 staining was performed at age 16 weeks. Positive cells were found in *Wfs1*$^{-/-}$ *A*^{y}*/a* islets (**s**), but not in islets from other mice. Scale bar, 50 nm

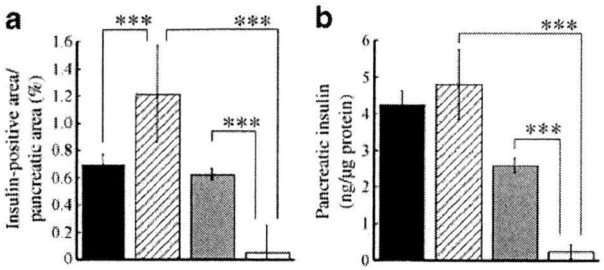

Fig. 4 Insulin-positive areas and insulin content of pancreases. **a** Ratios of total insulin-positive area to the entire pancreatic area were estimated for *Wfs1*$^{+/+}$ *a/a* (WT, black bars), *Wfs1*$^{+/+}$ *A*^{y}*/a* (hatched bars), *Wfs1*$^{-/-}$ *a/a* (grey bars) and the *Wfs1*$^{-/-}$ *A*^{y}*/a* (white bars) mice at age 24 weeks. At least five sections from each mouse were prepared and examined. Data are means±SE from four animals for each group. ***$p<0.001$. **b** Insulin contents extracted from whole pancreases of WT, *Wfs1*$^{+/+}$ *A*^{y}*/a*, *Wfs1*$^{-/-}$ *a/a* and *Wfs1*$^{-/-}$ *A*^{y}*/a* mice (key as above) at age 24 weeks (means±SE, $n=7$). ***$p<0.001$

24 weeks of age, whereas glucagon-positive alpha cells and somatostatin-positive delta cells were preserved (Fig. 3h, l). This selective beta cell loss was due to apoptotic cell death as indicated by caspase-3 activation in islets of 16-week-old mice (Fig. 3p–s).

Ultrastructural analysis We performed ultrastructural analyses of pancreatic beta cells from 12-week-old mice using electron microscopy. The beta cells were distinguished from alpha and delta cells by the appearance of their secretory granules. The beta cell granules had a white halo, not evident in alpha and delta cell granules.

In *A*^{y}*/a* mice pancreatic beta cells, rough ER was well developed and structurally indistinguishable from that of WT mice (Fig. 5a, b, e, f). In *Wfs1*$^{-/-}$ *a/a* mice, ER was dilated and beta cell secretory granules were electron-lucent in some pancreatic beta cells (Fig. 5c, g). In contrast, in *Wfs1*$^{-/-}$ *A*^{y}*/a* mice, ER was severely dilated in almost all pancreatic beta cells and secretory granules were reduced in size and electron density (Fig. 5d, h). In addition, mitochondrial swelling was observed in these beta cells. ER abnormality appears to be a common finding in rodent models of ER stress-related beta cell failure [26, 29, 30]. Riggs et al. reported similar findings in their beta cell-specific *Wfs1* knockout mouse [22]. Changes were milder in their mice than in our *Wfs1*$^{-/-}$ *A*^{y}*/a* mice and no mitochondrial abnormalities were mentioned. The difference may represent different stages of the same process.

Unfolded protein response in pancreatic islets of obese and Wfs1$^{-/-}$ *mice* Our group and others have shown that *Wfs1*$^{-/-}$ beta cells are susceptible to ER stress and that WFS1 deficiency itself evokes the UPR [15, 20, 22]. If insulin resistance induces ER stress in pancreatic beta cells via increased demand for insulin biosynthesis and secretion, beta cell death would presumably be accelerated in *Wfs1*$^{-/-}$ mice that become insulin-resistant. To examine this possibility, we first analysed WFS1 protein levels and the UPR in beta cells under insulin-resistant conditions. Western blot analysis at 12 weeks, when some mice were already hyperglycaemic, but more than half remained essentially normoglycaemic (Fig. 1b), revealed WFS1 protein levels to be increased in obese *Wfs1*$^{+/+}$ *A*^{y}*/a* murine islets as compared with those in *Wfs1*$^{+/+}$ a/a (WT) mice (Fig. 6a). Levels of ER chaperones 94 kDa glucose-regulated protein (GRP94) and 78 kDa glucose-regulated protein (GRP78) were also apparently increased in *Wfs1*$^{+/+}$ *A*^{y}*/a* and *Wfs1*$^{-/-}$ *a/a* mice as compared

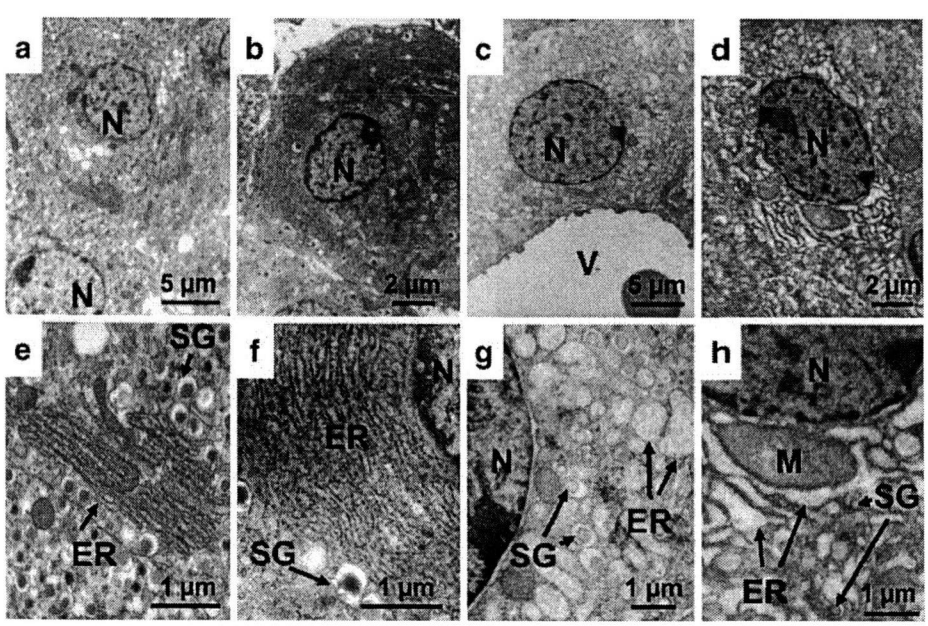

Fig. 5 Electron micrograph of pancreatic beta cells. Ultrastructural analysis using electron microscopy was performed on islets from *Wfs1*$^{+/+}$ *a/a* (WT) (**a**, **e**), *Wfs1*$^{+/+}$ *A*^{y}*/a* (**b**, **f**), *Wfs1*$^{-/-}$ *a/a* (**c**, **g**) and *Wfs1*$^{-/-}$ *A*^{y}*/a* mice (**d**, **h**) at age 12 weeks. Magnification was as shown, i.e. lower (**a–d**) and higher (**e–h**). M, mitochondrion; N, nucleus; SG, secretory granule; V, blood vessel

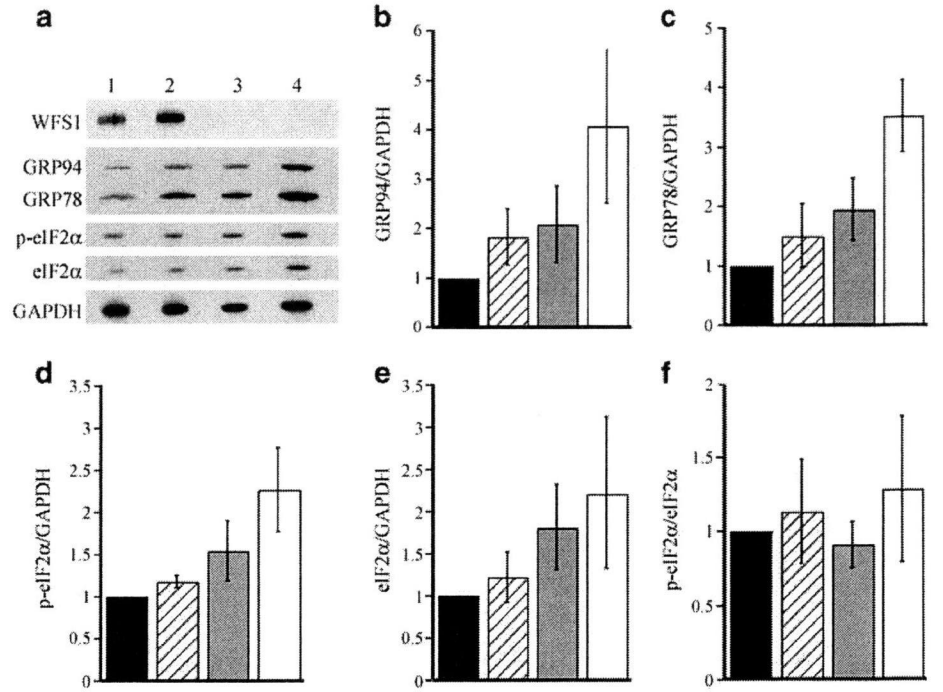

Fig. 6 Unfolded protein responses of pancreatic islets. **a** Isolated murine islets were subjected to SDS/PAGE and blotted using antibodies directed against WFS1 (N-terminus), C-terminal lys-asp-glu-leu (GRP94, GRP78), eIF2α, phosphorylated eIF2α (p-eIF2α) and glyceraldehyde 3-phosphate dehydrogenase (GAPDH). Lane 1, *Wfs1*$^{+/+}$ *a/a* (WT); lane 2, *Wfs*$^{+/+}$ *A*^{y}*/a;* lane 3, *Wfs*$^{-/-}$ *a/a*; lane 4, *Wfs*$^{-/-}$ *A*^{y}*/a*. The blot is representative of experiments repeated three times. **b–f** Summary of respective protein/GAPDH levels from three independent experiments. Data (means±SE) are expressed relative to those of the *Wfs1*$^{+/+}$ *a/a* (WT) islet preparation. Although the differences did not reach statistical significance, the UPR tended to be enhanced in *Wfs*$^{+/+}$ *A*^{y}*/a* (hatched bars) and *Wfs*$^{-/-}$ *a/a* (grey bars) mice as compared with the WT (*Wfs*$^{+/+}$ *a/a)* (black bars) mice, and appeared to be further enhanced in *Wfs*$^{-/-}$ *A*^{y}*/a* (white bars) mice. Experiments were performed using 12-week-old mice

with WT mice (Fig. 6a–c). Therefore, ER stress had been triggered in *A*^{y}*/a* and *Wfs1*$^{-/-}$ mice. In *Wfs1*$^{-/-}$ *A*^{y}*/a* mice, levels of these ER chaperones appeared to be further increased (Fig. 6a–c). Phosphorylation of the translation initiation factor-2, subunit α (eIF2α) attenuates protein translation under ER stress conditions. Similar changes were observed in total eIF2α protein and phosphorylated eIF2α amounts in the islets of *Wfs1*$^{+/+}$ *A*^{y}*/a*, *Wfs1*$^{-/-}$ *a/a* and *Wfs1*$^{-/-}$ *A*^{y}*/a* mice (Fig. 6a, d–f). We also measured *Grp78* (also known as *Hspa5*), *Grp94* (also known as *Hsp90b1*) and spliced *Xbp1* mRNA expression in 8-week-old mice islets. A similar trend was observed, although changes were less prominent at this age (ESM Fig. 2). These data suggest that *A*^{y}*/a* murine islets are exposed to ER stress and that increased ER stress is among the likely causes of rapid and prominent beta cell apoptosis in *Wfs1*$^{-/-}$ *A*^{y}*/a* murine islets.

Pioglitazone prevented beta cell loss and diabetes in Wfs1$^{-/-}$ *A*^{y}*/a mice* Our observations suggest that beta cell overload markedly accelerates beta cell death and diabetes development in *Wfs1*$^{-/-}$ *a/a* mice. Therefore, we attempted to reduce this beta cell overload, which is likely to be due to obesity-associated insulin resistance, with pioglitazone treatment. Mice were allowed free access to normal chow containing 0.01% pioglitazone immediately after weaning (4 weeks of age). The average dose of pioglitazone was estimated to be 15 mg kg^{-1} day^{-1}.

Pioglitazone ameliorated insulin resistance as assessed by the non-fasting insulin levels in *Wfs1*$^{+/+}$ *A*^{y}*/a* mice (mean non-fasting insulin without pioglitazone 513.5± 49.9 pmol/l, n=13 vs with pioglitazone 326.9±61.0 pmol/l, n=7, p<0.05) at 12 weeks of age. Serum triacylglycerol levels were also markedly improved (Fig. 7). The *Wfs1*$^{-/-}$ *A*^{y}*/a* mice gained more weight with pioglitazone treatment. As early as 7 weeks of age, *Wfs1*$^{-/-}$ *A*^{y}*/a* mice treated with pioglitazone were heavier (28.7±0.7 g, n=11) than *Wfs1*$^{+/+}$ *A*^{y}*/a* (25.5±0.7 g, n=15, p<0.01) and *Wfs1*$^{-/-}$ *A*^{y}*/a* (26.0± 0.4 g, n=20, p<0.01) mice fed normal chow (Fig. 8a). Despite the increased body weight, pioglitazone prevented diabetes development. Average non-fasted blood glucose levels were significantly lower in pioglitazone-treated *Wfs1*$^{-/-}$ *A*^{y}*/a* mice than in untreated *Wfs1*$^{-/-}$ *A*^{y}*/a* mice (12.9±0.9 vs 20.5±1.9 mmol/l, p<0.002) at 16 weeks (Fig. 8b). Histological analyses revealed pancreatic beta cells to be very well preserved in pioglitazone-treated *Wfs1*$^{-/-}$ *A*^{y}*/a* mice (Fig. 8c–f).

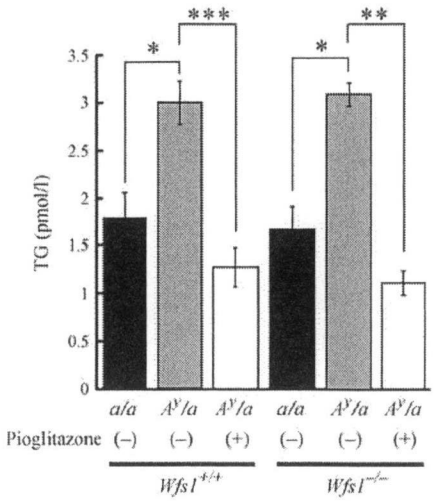

Fig. 7 Serum triacylglycerol (TG) levels with/without pioglitazone. Serum triacylglycerol levels were measured in 12-week-old mice. After weaning (4 weeks of age), the mice were fed standard mouse chow with/without 0.01% pioglitazone. Values are means±SE from three to five mice. *$p<0.05$, **$p<0.01$, ***$p<0.001$

Pioglitazone did not suppress the UPR To investigate whether pioglitazone treatment reduces ER stress in pancreatic beta cells, we examined UPR activation by Western blot analysis using isolated murine islets. Interestingly and unexpectedly, pioglitazone did not reduce either ER chaperones or eIF2α levels/phosphorylation in *Wfs1*$^{-/-}$ *a/a* and *Wfs1*$^{-/-}$ *A*^{y}*/a* mice (Fig. 9a, ESM Fig. 3). Similar results were obtained for spliced *Xbp1*, *Grp78*, *Grp94* and *Chop* (also known as *Ddit3*) mRNA expression in 8-week-old mice islets (ESM Fig. 2).

Electron microscopic examination revealed markedly improved ER appearance in *Wfs1*$^{-/-}$ *A*^{y}*/a* pancreatic beta cells after pioglitazone treatment (Fig. 9b–e, see also Fig. 5). Without the treatment, almost all beta cells had markedly distended ER (Fig. 9b, c). However, after the treatment, the ER distension was markedly reduced and some beta cells appeared to be normal (Fig. 9d, e), although heterogeneity was observed among the cells.

Discussion

Here we demonstrated that *Wfs1*$^{-/-}$ *A*^{y}*/a* mice on a C57BL/6J background develop early-onset insulin-deficient diabetes mellitus as early as 6 weeks of age and that most are overtly diabetic by the 16th week, whereas neither *Wfs1*-deficient *Wfs1*$^{-/-}$ *a/a* nor obese agouti yellow (*Wfs1*$^{+/+}$ *A*^{y}*/a*) mice had developed overt diabetes by the 24th week. In *Wfs1*$^{-/-}$ *A*^{y}*/a* murine islets, beta cell mass was dramatically decreased due to increased beta cell apoptosis. WFS1 protein clearly plays a pivotal role in beta cell survival.

Our previous study had demonstrated that approximately half of *Wfs1*$^{-/-}$ mice develop diabetes when they have the hybrid genetic background of C57BL/6J and 129Sv, while. unexpectedly with the C57BL/6J background, there is no apparent increase in blood glucose levels even at 36 weeks [15]. Because beta cells of *Wfs1*$^{-/-}$ mice were also shown to be susceptible to ER stress in ex-vivo experiments and cultured cells [15, 21], we sought to test this in the in vivo model.

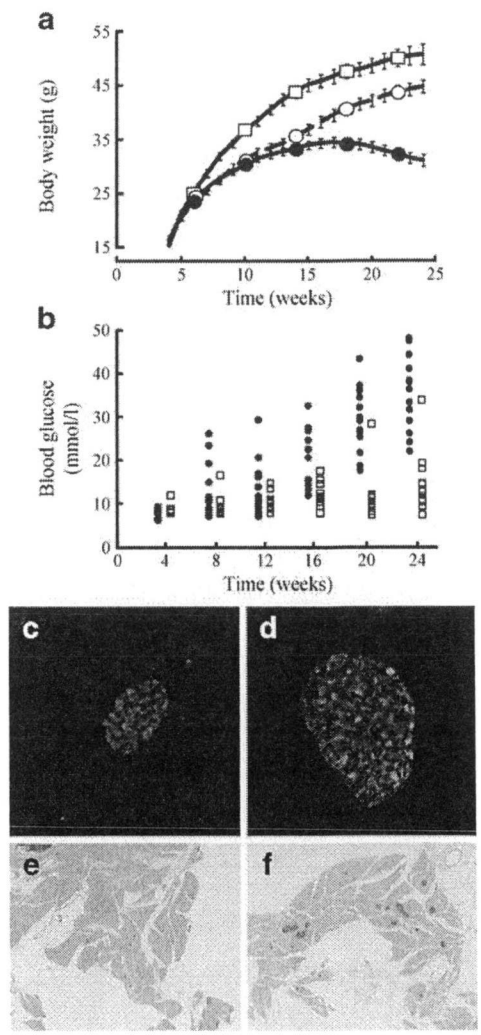

Fig. 8 Pioglitazone prevents diabetes and beta cell loss. The standard mouse chow with 0.01% pioglitazone was started at 4 and continued until 24 weeks of age in *Wfs1*$^{-/-}$ *A*^{y}*/a* mice. **a** Graph showing body weight changes (means±SE, $n=11–20$) and (**b**) non-fasted blood glucose levels ($n=11–16$). Black circles, *Wfs1*$^{-/-}$ *A*^{y}*/a* mice without treatment; squares, *Wfs1*$^{-/-}$ *A*^{y}*/a* mice with pioglitazone treatment; white circles, control *Wfs1*$^{+/+}$ *A*^{y}*/a* mice. **c** Insulin (green) and glucagon (red) were stained in pancreatic sections from *Wfs1*$^{-/-}$ *A*^{y}*/a* mice and (**d**) from pioglitazone-treated *Wfs1*$^{-/-}$ *A*^{y}*/a* mice at 24 weeks of age. **e** Insulin (brown) was stained in pancreatic sections from *Wfs1*$^{-/-}$ *A*^{y}*/a* mice and (**f**) from pioglitazone-treated *Wfs1*$^{-/-}$ *A*^{y}*/a* mice at 24 weeks of age

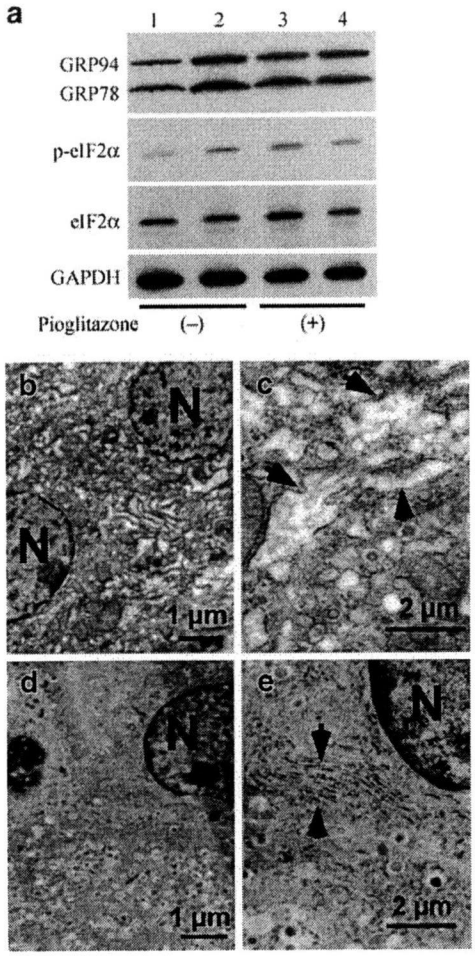

Fig. 9 Unfolded protein responses and ultrastructural changes in beta cells after pioglitazone treatment. **a** *Wfs1*$^{-/-}$ *a/a* (lanes 1, 3) and *Wfs1*$^{-/-}$ *A*^{y}*/a* (lanes 2, 4) mice were fed standard mouse chow with/without 0.01% pioglitazone after weaning (4 weeks of age). Isolated murine islets at 12 weeks of age were subjected to SDS/PAGE and blotted using antibodies directed against WFS1 (N-terminus), C-terminal lys-asp-glu-leu (GRP94, GRP78), eIF2α, phosphorylated eIF2α (p-eIF2α) and glyceraldehyde 3-phosphate dehydrogenase (GAPDH). The blot is representative of three independent experiments. Densitometric quantification of these results is presented in ESM Fig. 3). Electron micrographs of islets from *Wfs1*$^{-/-}$ *A*^{y}*/a* mice (12-week-old) without (**b**, **c**) or with (**d**, **e**) pioglitazone treatment. Arrows, ER; N, nucleus

The *A*^{y}*/a* mouse is a genetic model of mild obesity/insulin resistance with compensatory beta cell hyperplasia [31] (Figs 1 and 3). Increased demand for insulin biosynthesis and secretion has been thought to cause ER stress in pancreatic beta cells, and here, in fact, we demonstrated, in *A*^{y}*/a* murine islets, that ER chaperone expression was apparently increased at 12 weeks of age (Fig. 6). Similar results have been demonstrated in another insulin-resistant mouse model [7]. In addition, WFS1 protein levels were also increased (Fig. 6a). Our group and others have shown WFS1 protein levels to be upregulated by ER stress [19, 20, 35]. These data suggest that increased insulin demand under insulin-resistant conditions produces chronic ER stress in beta cells. In addition, NEFA, which are elevated in these insulin-resistant models, may also contribute to the activation of UPR [32]. In this regard, Lipson et al. recently demonstrated that hyperglycaemia activates inositol-requiring protein-1 (IRE1)α, an ER-resident transmembrane protein kinase regulating UPR in beta cells. Although IRE1α activation by transient hyperglycaemia is beneficial to beta cells, chronically sustained hyperglycaemia causes ER stress and suppresses insulin gene expression [36]. Glucose regulation of the UPR has also been reported [37].

Dramatically decreased beta cell numbers in *Wfs1*$^{-/-}$ *A*^{y}*/a* mice suggest that increased insulin demand triggers pancreatic beta cell apoptosis in *Wfs1*-deficient mice. ER stress induces WFS1 protein production and lack of this protein itself enhances the UPR [15, 19–21]. This was true in our mice (Fig. 6), with the UPR apparently further enhanced in mildly obese *Wfs1*$^{-/-}$ *A*^{y}*/a* mice. These data support the hypothesis that beta cell loss in Wolfram syndrome is, at least partly, caused by increased ER stress in beta cells. Although the precise function of ER-resident WFS1 protein remains unknown, our overall results suggest that this protein is likely to protect beta cells from ER stress-induced apoptosis and that Wolfram syndrome is an ER stress-related disease.

In patients with type 2 diabetes, very gradual, but progressive beta cell loss is caused by many factors, both genetic and acquired. One well-established mechanism of acquired beta cell loss is oxidative stress, which appears to be a major mediator of glucotoxicity [38]. We observed 4-hydroxy-2-nonenal-modified protein, an oxidative stress marker, in *Wfs1*$^{-/-}$ *A*^{y}*/a* murine islets at age 16 weeks (data not shown), suggesting that oxidative stress is also involved in beta cell apoptosis. Oxidative stress is likely to have been secondary to chronic hyperglycaemia because most *Wfs1*$^{-/-}$ *A*^{y}*/a* mice had developed hyperglycaemia by this age (Fig. 1b). In *Wfs1*$^{-/-}$ *A*^{y}*/a* mice, the vicious cycle associated with ER stress and oxidative stress probably exacerbates beta cell apoptosis. In this regard, it is again worth emphasising that insulin resistance induces ER stress in pancreatic beta cells [7]. Currently, we do not know the full extent of ER stress involvement in beta cell failure in human type 2 diabetes. However, it is possible that this vicious cycle associated with ER stress and oxidative stress plays an important role in beta cell deterioration [39].

Pioglitazone treatment almost completely prevented the development of diabetes and beta cell loss in *Wfs1*$^{-/-}$ *A*^{y}*/a* mice. One simple explanation is that insulin resistance was ameliorated by pioglitazone treatment, reducing ER stress in pancreatic beta cells and preventing beta cell death.

However, the mechanism may not be so simple. Unexpectedly, the UPR, represented by ER chaperone expression, was not significantly reduced (Fig. 9a, ESM Figs 2 and 3) to the extent that we expected from the remarkable level of diabetes prevention. Because the UPR is a protective response against ER stress, an apoptotic pathway may have been preferentially suppressed under these conditions. Several pathways are reportedly involved in ER stress-induced apoptosis, including the C/EBP-homologous protein (CHOP), the IRE1–TNF receptor-associated factor 2 (TRAF2)–apoptosis signal-regulating kinase 1 (ASK1), and the caspase 12 pathways [40]. The precise mechanism whereby pioglitazone prevented apoptosis in beta cells awaits determination. The beta cell protection exerted by thiazolidinediones including pioglitazone has been demonstrated in other rodent models [41, 42] and also in humans [43]. Although the precise mechanisms are not fully understood, one possibility is an indirect action through improvements in systemic glucose and lipid metabolism. Another mechanism involves direct actions on pancreatic beta cells [44]. Recent reports have demonstrated that thiazolidinediones directly improve beta cell function [45], ameliorate lipotoxicity [46] and prevent beta cell apoptosis [47, 48]. In *Wfs1*$^{-/-}$ *A*^{y}*/a* mice, direct protective effects, as well as indirect effects, are likely to be exerted. Elucidation of the mechanism whereby pioglitazone directly protects beta cells against apoptosis in *Wfs1*$^{-/-}$ *A*^{y}*/a* mice would provide insights into the mechanism of beta cell death in patients with Wolfram syndrome, as well as the function of WFS1 protein in beta cells.

This is one of a few good models showing that one genetic defect predisposes beta cells to profound failure upon ER stress induced by systemic insulin resistance [30, 49]. Our findings are important for the understanding of the molecular pathophysiology of Wolfram syndrome. In addition, a common process may be involved in conventional type 2 diabetes patients, whose beta cells decrease very slowly but progressively. In this context, a recent report has confirmed that common variants in the *WFS1* gene confer risk of type 2 diabetes [50]. Therefore knowledge from this model would help us to understand the mechanisms of, and to develop a way of preventing beta cell loss in patients with conventional type 2 diabetes mellitus.

Acknowledgements We thank M. Nishimura (Nagoya University Graduate School of Medicine) for kindly providing C57BL/6J*HamSlc*-A^{y} mice. This study was supported in part by Grants-in-Aid for Scientific Research (grant no16390096, 18390103 and 20390093 to Y. Tanizawa) from the Ministry of Education, Culture, Sports, Science and Technology of Japan, grant no. 16790510 (to K. Ueda) from the Japan Society for the Promotion of Science, grant H16-genome-003 (to Y. Oka and Y. Tanizawa) from the Ministry of Health, Labour and Welfare of Japan, and a grant from the Takeda Science Foundation (to Y. Tanizawa).

Duality of interest The authors declare that there is no duality of interest associated with this manuscript.

References

1. Rhodes CJ (2005) Type 2 diabetes—a matter of beta-cell life and death? Science 307:380–384
2. Butler AE, Janson J, Bonner-Weir S, Ritzel R, Rizza RA, Butler PC (2003) Beta-cell deficit and increased beta-cell apoptosis in humans with type 2 diabetes. Diabetes 52:102–110
3. Sakuraba H, Mizukami H, Yagihashi N, Wada R, Hanyu C, Yagihashi S (2002) Reduced beta-cell mass and expression of oxidative stress-related DNA damage in the islet of Japanese Type II diabetic patients. Diabetologia 45:85–96
4. Poitout V, Robertson RP (2008) Glucolipotoxicity: fuel excess and beta-cell dysfunction. Endocr Rev 29:351–366
5. Eizirik DL, Cardozo AK, Cnop M (2008) The role for endoplasmic reticulum stress in diabetes mellitus. Endocr Rev 29:42–61
6. Marchetti P, Bugliani M, Lupi R et al (2007) The endoplasmic reticulum in pancreatic beta cells of type 2 diabetes patients. Diabetologia 50:2486–2494
7. Laybutt DR, Preston AM, Akerfeldt MC et al (2007) Endoplasmic reticulum stress contributes to beta cell apoptosis in type 2 diabetes. Diabetologia 50:752–763
8. Barrett TG, Bundey SE (1997) Wolfram (DIDMOAD) syndrome. J Med Genet 34:838–841
9. Barrett TG, Bundey SE, Macleod AF (1995) Neurodegeneration and diabetes: UK nationwide study of Wolfram (DIDMOAD) syndrome. Lancet 346:1458–1463
10. Karasik A, O'Hara C, Srikanta S et al (1989) Genetically programmed selective islet beta-cell loss in diabetic subjects with Wolfram's syndrome. Diabetes Care 12:135–138
11. Inoue H, Tanizawa Y, Wasson J et al (1998) A gene encoding a transmembrane protein is mutated in patients with diabetes mellitus and optic atrophy (Wolfram syndrome). Nat Genet 20:143–148
12. Strom TM, Hortnagel K, Hofmann S et al (1998) Diabetes insipidus, diabetes mellitus, optic atrophy and deafness (DIDMOAD) caused by mutations in a novel gene (wolframin) coding for a predicted transmembrane protein. Hum Mol Genet 7:2021–2028
13. Takeda K, Inoue H, Tanizawa Y et al (2001) WFS1 (Wolfram syndrome 1) gene product: predominant subcellular localization to endoplasmic reticulum in cultured cells and neuronal expression in rat brain. Hum Mol Genet 10:477–484
14. Hofmann S, Philbrook C, Gerbitz KD, Bauer MF (2003) Wolfram syndrome: structural and functional analyses of mutant and wild-type wolframin, the WFS1 gene product. Hum Mol *Genet* 12:2003–2012
15. Ishihara H, Takeda S, Tamura A et al (2004) Disruption of the WFS1 gene in mice causes progressive beta-cell loss and impaired stimulus-secretion coupling in insulin secretion. Hum Mol Genet 13:1159–1170
16. Osman AA, Saito M, Makepeace C, Permutt MA, Schlesinger P, Mueckler M (2003) Wolframin expression induces novel ion channel activity in endoplasmic reticulum membranes and increases intracellular calcium. J Biol Chem 278:52755–52762

17. Takei D, Ishihara H, Yamaguchi S et al (2006) WFS1 protein modulates the free Ca^{2+} concentration in the endoplasmic reticulum. FEBS Lett 580:5635–5640
18. Zatyka M, Ricketts C, da Silva Xavier G et al (2008) Sodium-potassium ATPase 1 subunit is a molecular partner of Wolframin, an endoplasmic reticulum protein involved in ER stress. Hum Mol Genet 17:190–200
19. Fonseca SG, Fukuma M, Lipson KL et al (2005) WFS1 is a novel component of the unfolded protein response and maintains homeostasis of the endoplasmic reticulum in pancreatic beta-cells. J Biol Chem 280:39609–39615
20. Ueda K, Kawano J, Takeda K et al (2005) Endoplasmic reticulum stress induces Wfs1 gene expression in pancreatic beta-cells via transcriptional activation. Eur J Endocrinol 153:167–176
21. Yamada T, Ishihara H, Tamura A et al (2006) WFS1-deficiency increases endoplasmic reticulum stress, impairs cell cycle progression and triggers the apoptotic pathway specifically in pancreatic beta-cells. Hum Mol Genet 15:1600–1609
22. Riggs AC, Bernal-Mizrachi E, Ohsugi M et al (2005) Mice conditionally lacking the Wolfram gene in pancreatic islet beta cells exhibit diabetes as a result of enhanced endoplasmic reticulum stress and apoptosis. Diabetologia 48:2313–2321
23. Schroder M, Kaufman RJ (2005) The mammalian unfolded protein response. Annu Rev Biochem 74:739–789
24. Ron D, Walter P (2007) Signal integration in the endoplasmic reticulum unfolded protein response. Nat Rev Mol Cell Biol 8:519–529
25. Scheuner D, Kaufman RJ (2008) The unfolded protein response: a pathway that links insulin demand with beta-cell failure and diabetes. Endocr Rev 29:317–333
26. Harding HP, Zeng H, Zhang Y et al (2001) Diabetes mellitus and exocrine pancreatic dysfunction in $perk^{-/-}$ mice reveals a role for translational control in secretory cell survival. Mol Cell 7:1153–1163
27. Delepine M, Nicolino M, Barrett T, Golamaully M, Lathrop GM, Julier C (2000) *EIF2AK3*, encoding translation initiation factor 2-alpha kinase 3, is mutated in patients with Wolcott-Rallison syndrome. Nat Genet 25:406–409
28. Scheuner D, Song B, McEwen E et al (2001) Translational control is required for the unfolded protein response and in vivo glucose homeostasis. Mol Cell 7:1165–1176
29. Wang J, Takeuchi T, Tanaka S et al (1999) A mutation in the insulin 2 gene induces diabetes with severe pancreatic beta-cell dysfunction in the Mody mouse. J Clin Invest 103:27–37
30. Scheuner D, Vander MD, Song B et al (2005) Control of mRNA translation preserves endoplasmic reticulum function in beta cells and maintains glucose homeostasis. Nat Med 11:757–764
31. Wolff GL, Roberts DW, Mountjoy KG (1999) Physiological consequences of ectopic agouti gene expression: the yellow obese mouse syndrome. Physiol Genomics 11:151–163
32. Cunha DA, Hekerman P, Ladrière L et al (2008) Initiation and execution of lipotoxic ER stress in pancreatic beta-cells. J Cell Sci 121:2308–2318
33. Usui S, Hara Y, Hosaki S, Okazaki M (2002) A new on-line dual enzymatic method for simultaneous quantification of cholesterol and triglycerides in lipoproteins by HPLC. J Lipid Res 43:805–814
34. Oka Y, Asano T, Shibasaki Y, Kasuga M, Kanazawa Y, Takaku F (1988) Studies with antipeptide antibody suggest the presence of at least two types of glucose transporter in rat brain and adipocyte. J Biol Chem 263:13432–13439
35. Yamaguchi S, Ishihara H, Tamura A (2004) Endoplasmic reticulum stress and N-glycosylation modulate expression of WFS1 protein. Biochem Biophys Res Commun 325:250–256
36. Lipson KL, Fonseca SG, Ishigaki S et al (2006) Regulation of insulin biosynthesis in pancreatic beta cells by an endoplasmic reticulum-resident protein kinase IRE1. Cell Metab 4:245–254
37. Elouil H, Bensellam M, Guiot Y et al (2007) Acute nutrient regulation of the unfolded protein response and integrated stress response in cultured rat pancreatic islets. Diabetologia 50:1442–1452
38. Robertson RP, Harmon JS (2006) Diabetes, glucose toxicity, and oxidative stress: a case of double jeopardy for the pancreatic islet beta cell. Free Radic Biol Med 41:177–184
39. Malhotra JD, Kaufman RJ (2007) Endoplasmic reticulum stress and oxidative stress: a vicious cycle or a double-edged sword? Antioxid Redox Signal 9:2277–2293
40. Yoshida H (2007) ER stress and diseases. FEBS J 274:630–658
41. Ishida H, Takizawa M, Ozawa S (2004) Pioglitazone improves insulin secretory capacity and prevents the loss of beta-cell mass in obese diabetic db/db mice: possible protection of beta cells from oxidative stress. Metabolism 53:488–494
42. Diani AR, Sawada G, Wyse B, Murray FT, Khan M (2004) Pioglitazone preserves pancreatic islet structure and insulin secretory function in three murine models of type 2 diabetes. Am J Physiol Endocrinol Metab 286:116–122
43. Dormandy JA, Charbonnel B, Eckland DJ et al (2005) Secondary prevention of macrovascular events in patients with type 2 diabetes in the PROactive Study (PROspective pioglitAzone Clinical Trial In macroVascular Events): a randomised controlled trial. Lancet 366:1279–1289
44. Rosen ED, Kulkarni RN, Sarraf P et al (2003) Targeted elimination of peroxisome proliferator-activated receptor gamma in beta cells leads to abnormalities in islet mass without compromising glucose homeostasis. Mol Cell Biol 23:7222–7229
45. Kim HI, Ahn YH (2004) Role of peroxisome proliferator-activated receptor-gamma in the glucose-sensing apparatus of liver and beta-cells. Diabetes 53(Suppl 1):S60–S65
46. Saitoh Y, Chun-ping C, Noma K et al (2008) Pioglitazone attenuates fatty acid-induced oxidative stress and apoptosis in pancreatic beta-cells. Diabetes Obes Metab 10:564–573
47. Lin CY, Gurlo T, Haataja L, Hsueh WA, Butler PC (2005) Activation of peroxisome proliferator-activated receptor-gamma by rosiglitazone protects human islet cells against human islet amyloid polypeptide toxicity by a phosphatidylinositol 3′-kinase-dependent pathway. J Clin Endocrinol Metab 90:6678–6686
48. Zeender E, Maedler K, Bosco D et al (2004) Pioglitazone and sodium salicylate protect human beta-cells against apoptosis and impaired function induced by glucose and interleukin-1beta. J Clin Endocrinol Metab 89:5059–5066
49. Huang C, Lin C, Haataja L et al (2007) High expression rates of human islet amyloid polypeptide induce endoplasmic reticulum stress-mediated beta-cell apoptosis, a characteristic of humans with type 2 but not type 1 diabetes. Diabetes 56:2016–2027
50. Sandhu MS, Weedon MN, Fawcett KA et al (2007) Common variants in *WFS1* confer risk of type 2 diabetes. Nat Genet 39:951–953

Atherosclerosis 206 (2009) 168–172

Contents lists available at ScienceDirect

Atherosclerosis

journal homepage: www.elsevier.com/locate/atherosclerosis

Carotid arterial elasticity is a sensitive atherosclerosis value reflecting visceral fat accumulation in obese subjects

Ai Tokita[a], Yasushi Ishigaki[a], Hisashi Okimoto[a], Hideyuki Hasegawa[c], Yoshiro Koiwa[d], Makoto Kato[e], Hisamitsu Ishihara[a], Yoshinori Hinokio[a], Hideki Katagiri[b], Hiroshi Kanai[c], Yoshitomo Oka[a,*]

[a] Division of Molecular Metabolism and Diabetes, Tohoku University Graduate School of Medicine, 2-1 Seiryo-machi, Aoba-ku, Sendai 980-8575, Japan
[b] Division of Advanced Therapeutics for Metabolic Diseases, Tohoku University Graduate School of Medicine, Japan
[c] Department of Electrical Engineering, Tohoku University Graduate School of Engineering, Tohoku University, Sendai, Japan
[d] Oizumi Memorial Hospital, Shiroishi, Japan
[e] Panasonic Shikoku Electronics Co., Ltd., Yokohama, Japan

ARTICLE INFO

Article history:
Received 30 August 2008
Received in revised form 29 January 2009
Accepted 30 January 2009
Available online 20 February 2009

Keywords:
Elasticity
Obesity
Ultrasound
Visceral adiposity
Early stage atherosclerosis

ABSTRACT

Background: We previously reported the arterial elasticity value we measured to reflect the characteristic features of vessel walls, and to possibly be useful for detecting early stage atherosclerosis in type 2 diabetes. Obesity, especially visceral adiposity, is well known to play a crucial role in the development of metabolic disorders and atherosclerosis. To assess whether arterial elasticity value reflects the effect of obesity on atherosclerosis, we examined the associations of obesity characteristics with atherosclerosis values including arterial elasticity, carotid intima–media thickness (IMT) and pulse wave velocity (PWV).
Methods: Three atherosclerosis values were measured in 78 obese subjects (body mass index ≥30). We investigated the associations of atherosclerosis values with obesity-related parameters including abdominal fat accumulation determined by computed tomography.
Results: Arterial elasticity values were positively related to established atherosclerosis values, carotid IMT and PWV, in obese subjects. Age, systolic blood pressure and hypertension also correlated with these atherosclerosis values. Single regression analysis showed all three atherosclerosis values to correlate significantly with visceral fat area. Intriguingly, visceral fat area is an independent variable affecting arterial elasticity, but not IMT or PWV. Furthermore, multiple regression analysis revealed that arterial elasticity correlates strongly with visceral fat area.
Conclusions: Arterial elasticity value we measure is a new parameter for evaluating atherosclerosis in subjects with visceral adiposity and more sensitive than the currently established atherosclerosis values, carotid IMT and PWV. Measuring arterial elasticity has the potential to reveal minute vascular changes, and may have broad clinical applications for evaluating early stage atherosclerosis.

Obesity has increased dramatically, becoming a global epidemic in recent decades [1]. Obesity is closely associated with the development of atherosclerosis [2], via rising incidences of metabolic disorders, including diabetes, dyslipidemia, hypertension, inflammation, and the prothrombotic state [3]. Furthermore, obesity is involved in sympathetic nerve activation as well as cardiac structural and functional adaptations [4], and is reportedly an independent cardiovascular risk factor [5]. Recent studies have shown that adipocytokines, such as PAI-1, TNF-α and adiponectin, play crucial roles in the development of metabolic disorders and atherosclerosis, in various tissues including the vasculature [6]. In particular, visceral fat accumulation, rather than the body mass index (BMI) or subcutaneous fat accumulation, was shown to be strongly associated with various obesity-related disorders [7], and is thus considered to be a major risk factor for cardiovascular disease [8]. Many studies have shown that increasing body weight is closely related to the surrogate markers associated with atherosclerosis, such as carotid intima–media thickness (IMT) and pulse wave velocity (PWV). In addition, visceral adiposity is reportedly related to atherosclerosis, which is determined by carotid IMT [9–13], coronary calcification [14] and arterial stiffness [15,16]. In some reports, this relationship persisted after adjustments for multiple linear regression analysis [12–15]. While visceral fat areas were correctly measured by computed tomography (CT) scans in few studies [12,15], abdominal ultrasound was employed in many

* Corresponding author. Tel.: +81 22 717 7611; fax: +81 22 717 7611.
E-mail address: oka-y@mail.tains.tohoku.ac.jp (Y. Oka).

0021-9150/$ – see front matter © 2009 Elsevier Ireland Ltd. All rights reserved.
doi:10.1016/j.atherosclerosis.2009.01.046

reports [9–11,13,14,16], which is often imprecise to determine visceral fat area. It has been widely recognized that non-invasive methods of evaluating atherosclerosis have limitations, such as slow changes in carotid IMT and the influence of blood pressure on PWV. Thus, an accurate and practical means of evaluating atherosclerosis is needed.

Recently, we developed a novel non-invasive method for measuring a change in thickness of multiple layers preset in arterial wall during a single heartbeat [17,18]. Briefly, multiple points were preset from the luminal surface to the adventitia of the posterior wall along an ultrasonic beam and the displacements at these preset points were estimated by applying the phased tracking method to the received echo. A layer was defined as being between two points. A minute change in thickness of the layer was obtained by subtraction of the displacements at these two points and then, the strain of the layer was obtained by dividing the change in thickness by the original thickness set at the end diastole. By changing the depth and applying the same procedure, the strains at multiple depths in arterial wall were obtained at constant intervals, usually 80 μm. This innovative phased tracking method enables us to evaluate regional characteristics of the artery in detail; during a single heartbeat these sites either deform easily in soft regions or there is little deformation in hard regions. We integrated changes in thickness, which we describe with the term "arterial elasticity". This "arterial elasticity" measurement is a promising approach to evaluating atherosclerosis [19,20]. Therefore, we applied this method to in vivo detection of regional changes in human carotid arterial walls. In a study of subjects with type 2 diabetes, carotid arterial elasticity correlated significantly with currently established values for atherosclerosis, such as carotid artery IMT and PWV. Intriguingly, in subjects with IMT <1.1 mm, who are classified as not having atherosclerosis as defined by IMT criteria, arterial elasticity correlated with the number of risk factors, i.e. diabetes, dyslipidemia, hypertension and smoking, suggesting that arterial elasticity has potential for detecting early stage atherosclerosis. It was also suggested that measuring arterial elasticity would allow evaluation of qualitative changes in the carotid arterial wall [21].

Herein, to assess whether the effect of obesity on atherosclerosis can be evaluated using arterial elasticity, we examined the associations of obesity characteristics with atherosclerosis values including arterial elasticity, carotid IMT and PWV. We further evaluated the impact of fat distribution on atherosclerosis.

1. Methods

1.1. Study subjects

The study subjects were recruited from among patients with BMI over 30 at Tohoku University Hospital. Patients with type 1 diabetes, renal failure (serum creatinine >2.0 mg/dL), severe heart failure (NYHA functional class 2–4), atrial fibrillation and peripheral arterial disease were excluded from the study. The study protocol was approved by the Tohoku University Institutional Review Board. Informed consent was obtained from each patient.

We used the following criteria for the diagnosis of metabolic disorders. Diabetes was defined as fasting blood glucose ≥7.0 mmol/dl (126 mg/dl) and/or hemoglobin A1c ≥6.5%, based on the definition proposed by the Japan Diabetes Society, or taking antidiabetic drugs including insulin. Dyslipidemia was defined as LDL cholesterol ≥3.6 mmol/dl (140 mg/dl) and/or triglyceride ≥1.7 mmol/l (150 mg/dl), based on the definition proposed by the Japan Atherosclerosis Society in 2007, or taking lipid-lowering drugs. The subjects whose systolic blood pressure (BP) ≥140 mmHg and/or diastolic BP ≥90 mmHg (Japanese Society of Hypertension guidelines 2004) or who were taking antihypertensive drugs were defined as having hypertension. The subjects who currently smoked were classified as current smokers.

1.2. Measurement of arterial wall elasticity

Real-time measurement of regional elasticity in the far wall of common carotid artery (CCA) was achieved based on a previously described method [22] with ultrasound diagnostic equipment (prototype system by Panasonic), which was specialized for measuring regional elasticity. With this system, an ultrasound beam sequentially scanned an artery along its length at 32 positions at intervals of 200 μm with a linear type 7.5-MHz probe.

Multiple points were preset from the luminal surface to the adventitia along each beam at constant intervals of 80 μm, and the displacements at these preset points were estimated by applying the phased tracking method to the received echo. A layer was defined as being between two points, where the distance between these two points (i.e. the thickness of the layer) was set at 320 μm. As shown in Fig. 1C, minute changes in thickness of the layer were obtained by subtraction of the displacements at these two points and then, the strain of the layer was obtained by dividing the change in thickness by the original thickness (320 μm) which was set at the end diastole. By changing the depth of the layer at intervals of 80 μm and applying the same procedure, the strains at multiple depths were obtained at intervals of 80 μm.

The elasticity of each layer was obtained from the maximal strain and the pulse pressure measured at the upper arm. The maximal strain is defined by the absolute value of difference between the maximum and minimum of the measured change in thickness, as shown in Fig. 1C, and the maximal strain was determined at each location, independent of time.

Using the above procedure, the elasticity was obtained at intervals of 80 μm in the direction of depth and 200 μm along its length, as shown in Fig. 1B. Regional elasticity values of multiple sites in each layer were displayed as shown in Fig. 1A and a mean regional elasticity value (kPa) of bilateral CCA was used for analysis.

1.3. Measurement of carotid artery intima–media thickness

IMT of the carotid arteries was measured using ultrasound diagnostic equipment (EUB-450, Hitachi Medico, Tokyo, Japan) with an electrical linear transducer (center-frequency of 7.5 MHz). By B-mode ultrasound, CCA, carotid bulb, and portions of the internal and external carotid arteries on both sides were scanned with the subject in the supine position. IMT was measured at a point on the far wall of the CCA, 1 cm proximal to the bifurcation [23], from the longitudinal scan plane that showed the intima–media boundaries most clearly.

1.4. Measurement of PWV

PWV values were measured using an automatic waveform analyzer (BP-203RPE; Colin Co., Komaki, Japan) [24]. Pulse waves were recorded on the right brachial artery and both posterior tibial arteries. The average PWV was calculated by dividing the arm–ankle distance by the pulse wave transmission time between these points on both sides.

1.5. Measurement of abdominal fat area

Abdominal subcutaneous and intra-abdominal fat areas were measured by CT scans with a SOMATOM Definition (Siemens AG., Munich, Germany) at the level of the fourth lumbar vertebra. The border of the intra-abdominal cavity was outlined on the CT image and the total area of visceral fat was measured at an attenuation range of −200 and −50 Hounsfield units [25].

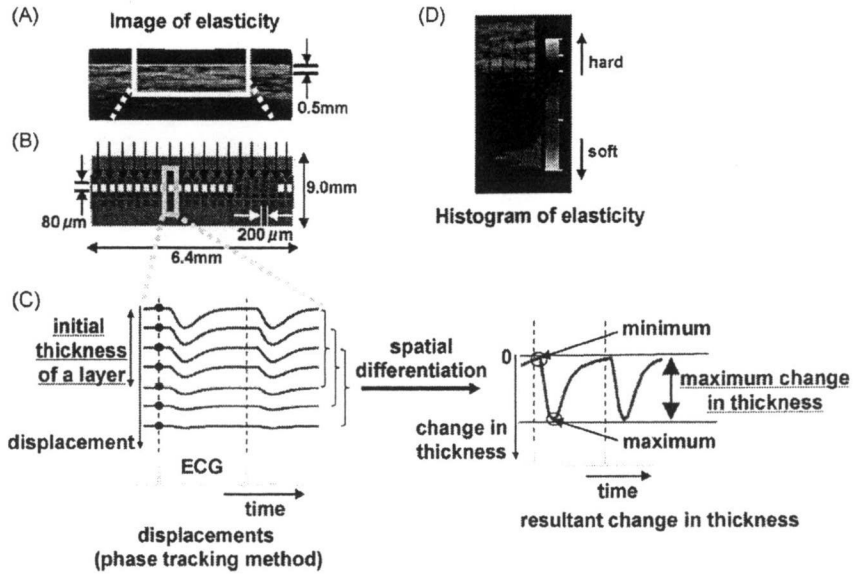

Fig. 1. Evaluation of carotid artery elasticity by phase tracking method. Arterial elasticity is displayed as a 2D cross-sectional color image, which is updated at every heartbeat (A). Multiple sites are preset from the luminal surface to the adventitia (113 depths × 32 beams per 9 mm × 6.4 mm scanned area) and elasticity in each module is measured by the phase tracking method (B). The arterial wall was divided into multiple layers with thicknesses set at 320 μm. The changes in thickness at each depth during the cardiac cycle are simultaneously obtained, and the maximum change in thickness corresponds to the elasticity in each module (C). The elasticity distribution is shown as a histogram (D).

1.6. Statistical analysis

Variables were compared using Pearson's regression analysis. Then, a multiple linear regression analysis was performed to evaluate the independent parameters that were significantly related to arterial elasticity. All data are expressed means ± S.D., and a p-value less than 0.05 was accepted as indicating statistical significance. All statistical analyses were performed using the Statistical Package for the Social Sciences version 13.0 (SPSS Japan Inc., Tokyo, Japan).

2. Results

The clinical characteristics of 78 subjects are shown in Table 1. Mean age is 41.0 ± 13.9 years, BMI 37.6 ± 7.2 (kg/m^2). Thus, the subjects were relatively young and categorized as having moderate, extreme or severe obesity according to Japanese guidelines.

To assess the clinical relevance of carotid artery elasticity in obese subjects, the arterial elasticity value was compared to atherosclerosis values obtained with currently established methods, carotid IMT and PWV. Arterial elasticity showed significant positive correlations with both carotid IMT ($r = 0.422$, $p < 0.01$) and PWV ($r = 0.360$, $p < 0.01$) in obese subjects (Fig. 2). Similar positive correlations among these three atherosclerosis values were observed in our previous results in subjects with type 2 diabetes [21]. The IMT value in this study was 0.61 ± 0.17 (range: 0.30–1.20) mm and PWV was 1396 ± 260 (range: 992–2117) cm/s, i.e. these obese subjects did not have advanced atherosclerosis, in contrast to the results in subjects with type 2 diabetes in our previous study (IMT: 0.94 ± 0.30 mm, PWV: 1703 ± 356 cm/s).

We then explored the association of carotid arterial elasticity with the clinical and demographic characteristics of these obese

Table 1
Subject characteristics.

Number	78
Age, years	41.0 ± 13.9
Gender (male), %	29.5
Body weight, kg	98.8 ± 24.2
BMI, kg/m^2	37.6 ± 7.2
Fasting blood glucose, mg/dl	121.3 ± 47.6
HbA1c, %	6.5 ± 1.8
Serum insulin μU/ml	17.8 ± 13.2
HOMA-R	4.5 ± 3.8
Systolic BP, mmHg	126.9 ± 14.4
Diastolic BP, mmHg	79.8 ± 10.7
Total cholesterol, mg/dl	208.2 ± 43.5
HDL cholesterol, mg/dl	45.8 ± 9.6
LDL cholesterol, mg/dl	132.6 ± 32.9
Triglyceride, mg/dl	184.1 ± 177.4
Uric acid, mg/dl	5.9 ± 1.5
Visceral fat area, cm^2	150.3 ± 55.7
Subcutaneous fat area, cm^2	405.7 ± 160.0
Diabetes, %	46.8
Dyslipidemia, %	60.3
Hypertension, %	48.7
Current smoker, %	28.0

Mean ± S.D.

Table 2
Associations between atherosclerosis values and subject characteristics.

Variables	r		
	Elasticity	IMT	PWV
Age	0.46**	0.44**	0.67**
Male	0.27*	0.24**	−0.086
Body weight	0.03	−0.075	−0.11
BMI	0.07	−0.06	0.045
Fasting blood glucose	0.14	0.032	0.14
HbA1c	−0.02	−0.036	0.0095
Total cholesterol	0.20	0.061	0.030
HDL cholesterol	−0.03	0.19	0.060
LDL cholesterol	0.15	0.034	−0.049
Triglyceride	−0.03	0.005	−0.040
Systolic BP	0.38**	0.27*	0.35**
Diastolic BP	0.28*	0.26*	0.047
Uric acid	0.15	0.10	−0.20
Diabetes	0.15	0.091	0.39**
Dyslipidemia	0.04	−0.11	0.037
Hypertension	0.37**	0.39**	0.51**

* $p < 0.05$.
** $p < 0.01$.

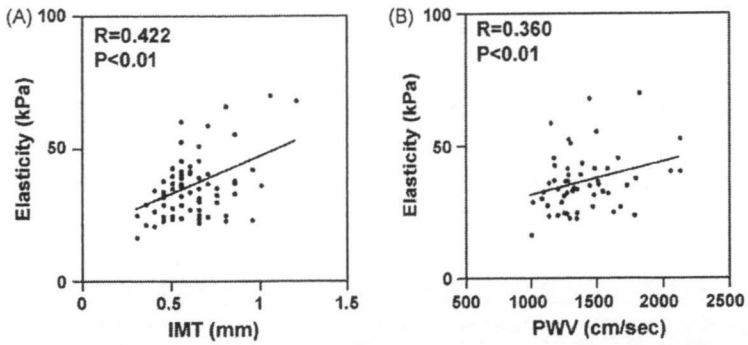

Fig. 2. Correlations of arterial elasticity with carotid IMT (A) and PWV (B) in obese subjects.

Table 3
Associations between each atherosclerosis value and fat distribution.

Variables	r		
	Elasticity	IMT	PWV
Visceral fat area	0.42**	0.25*	0.31*
Subcutaneous fat area	−0.066	−0.111	0.046

* $p<0.05$.
** $p<0.01$.

subjects. As shown in Table 2, arterial elasticity correlated with age ($r=0.46$, $p<0.01$), gender ($r=0.27$, $p<0.05$), BP, both systolic ($r=0.38$, $p<0.01$) and diastolic ($r=0.28$, $p<0.05$), and hypertension ($r=0.37$, $p<0.01$). Carotid IMT and PWV also showed similar associations with age, systolic BP and hypertension.

To evaluate whether fat distribution affects atherosclerosis in obese subjects, we performed a single regression analysis of atherosclerosis values with subcutaneous or visceral fat accumulation, as determined by CT scanning. Interestingly, visceral fat area correlated significantly with arterial elasticity as well as carotid IMT and PWV (Table 3), whereas subcutaneous fat area showed no apparent association with these three atherosclerosis values in the present study. Then, we performed multiple linear regression analysis with parameters related to atherosclerosis values, i.e. age, hypertension and visceral fat area (Tables 2 and 3), to search for independent variables affecting atherosclerosis values in obese subjects. As shown in Table 4, each atherosclerosis value is associated with age, indicating that age is also a strong atherosclerosis determinant in obese subjects. Intriguingly, the analysis revealed that visceral fat area is an independent variable showing a positive correlation with carotid arterial elasticity, but not carotid IMT or PWV. We next analyzed the results in a different way, to determine which of the atherosclerosis values is most strongly associated with visceral adiposity. Visceral fat area was significantly associated with both arterial elasticity and PWV, though the correlation with arterial elasticity was stronger (Table 5). These results suggest

Table 4
Multivariate adjustment for parameters related to atherosclerosis values.

Variables	Regression coefficient		
	Elasticity[a]	IMT[b]	PWV[c]
Age	0.30*	0.34**	0.52**
Visceral fat area	0.28**	0.075	−0.06
Hypertension	0.13	0.019	0.32*

[a] $R^2=0.32$.
[b] $R^2=0.25$.
[c] $R^2=0.47$.
* $p<0.05$
** $p<0.01$.

Table 5
Multivariate adjustment for parameters related to visceral fat area.

Variables	Regression coefficient	p
Elasticity	0.34	0.0041
IMT	0.034	0.77
PWV	0.22	0.047

$R^2=0.23$.

that arterial elasticity is an excellent parameter of atherosclerosis as compared with currently established atherosclerosis values and might reflect the cardiovascular risk of visceral adiposity.

3. Discussion

We measured two established atherosclerosis values, carotid IMT and PWV, in addition to "arterial elasticity", which was measured by a novel method, in this study. Similar to our previous results in subjects with type 2 diabetes [21], the arterial elasticity value was significantly associated with those of carotid IMT and PWV. These results raise the possibility of evaluating atherosclerosis in obese subjects with this novel method of measuring elasticity. The important finding of the present study is that arterial elasticity is a better measurement than either carotid IMT or PWV for evaluating the effect of visceral fat accumulation on atherosclerosis in obese subjects; the multiple linear regression analysis revealed that only carotid arterial elasticity, not carotid IMT or PWV, showed a positive correlation with visceral fat area.

In addition, our present results clearly shows that visceral adiposity rather than subcutaneous adiposity is an important factor affecting atherosclerosis in Japanese obese subjects with BMI over 30, since all three parameters for evaluating atherosclerosis, arterial elasticity, carotid IMT and PWV, were significantly associated with visceral fat area but not with subcutaneous fat area. Abdominal fat accumulation, especially visceral adiposity, is well known to play a crucial role in the development of metabolic syndrome [26], leading to atherosclerosis and ultimately cardiovascular disease [6]. Indeed, visceral adiposity determined by CT scanning was related to the incidence of coronary artery disease [8]. Furthermore, recent reports have shown several surrogate markers for atherosclerosis, such as carotid IMT [9–13] and arterial stiffness [15], to be associated with intra-abdominal fat accumulation in subjects without advanced atherosclerosis. Since obesity is increasing explosively world-wide, a practical and non-invasive method is urgently needed for early detection of atherosclerosis before serious cardiovascular events occur.

Herein, we have shown that our novel method of measuring arterial elasticity has potential for detecting early stage atherosclerosis in obese subjects. This ultrasonic method accurately tracks arterial wall movements based on both the phase and the

magnitude of demodulated signals, allowing instantaneous determination of the position of an object. With this method, it is possible to accurately detect small-amplitude velocity signals, less than a few micrometers, which are superimposed on arterial motion due to the heartbeat. Thus, the values obtained with this method reflect an important characteristic of vessel walls, i.e. arterial elasticity. We previously reported arterial elasticity to be a promising method of evaluating early stage atherosclerosis in subjects with type 2 diabetes [21]. Taken together with the present results in obese subjects, these finding indicate that measurement of arterial elasticity might be broadly applicable to evaluation of subjects with atherosclerosis-prone metabolic disorders.

This novel method also has potential for evaluating the elasticity distribution in vessel walls with high spatial resolution; the elasticity distribution is demonstrated as a histogram as shown in Fig. 1D. Properties of the histogram, such as deviation and the shape of the distribution, which were not used in this study, would provide additional information regarding qualitative changes in atherosclerosis. This possibility should be pursued in future investigations.

Several studies have examined which obesity-related values, including body weight, BMI, waist–hip ratio and abdominal fat accumulation, are closely associated with atherosclerosis values such as carotid IMT [27,28] and PWV [29]. However, comparisons among these atherosclerosis values were not conducted, i.e., which of the atherosclerosis values, IMT, PWV or elasticity, is most strongly associated with obesity-related values remains to be determined. This is the first report demonstrating arterial elasticity to have a stronger association with visceral fat area in obese subjects than the two most widely used atherosclerosis values, IMT and PWV.

The present study has several limitations. The study design was cross-sectional. Determination of whether arterial elasticity predicts cardiovascular events in the future thus awaits a prospective study. Another issue warranting further investigation is whether reducing visceral adiposity would improve arterial elasticity. Another important issue is that only approximately 30% of our study subjects were male. The difference in fat distribution by gender is well known, i.e. visceral adiposity is more frequently observed in males [30] and subcutaneous adiposity in females [25]. However, despite the female dominance in our subject group, the effect of visceral adiposity on arterial elasticity was confirmed by multiple regression analysis, implying a crucial role of visceral fat in atherosclerosis.

In conclusion, the present results indicate that arterial elasticity is a novel, sensitive parameter for evaluating atherosclerosis in obese subjects, potentially more useful than currently established atherosclerosis values. Measuring arterial elasticity hold promise of detecting minute vascular changes in early stage atherosclerosis, and may have broad clinical applications for evaluating atherosclerosis in subjects with metabolic disorders.

Acknowledgments

This work was supported by a Grant-in-Aid for Scientific Research (19591031) to Y. Ishigaki and the Global-COE Programs to Y. Oka from the Ministry of Education, Culture, Sports, Science and Technology of Japan. This work was also supported by a Grant-in-Aid for Research on Human Genome, Tissue Engineering (H17-genome-003) to Y. Oka. We thank Dr. T. Ohkubo for helpful suggestions on the statistical analysis. We also thank N. Tamura for technical support.

References

[1] Friedman JM. A war on obesity, not the obese. Science 2003;299:856–8.
[2] Yusuf S, Hawken S, Ounpuu S, et al. Obesity and the risk of myocardial infarction in 27,000 participants from 52 countries: a case-control study. Lancet 2005;366:1640–9.
[3] Eckel RH, Grundy SM, Zimmet PZ. The metabolic syndrome. Lancet 2005;365:1415–28.
[4] Klein S, Burke LE, Bray GA, et al. Clinical implications of obesity with specific focus on cardiovascular disease: a statement for professionals from the American Heart Association Council on Nutrition, Physical Activity, and Metabolism: endorsed by the American College of Cardiology Foundation. Circulation 2004;110:2952–67.
[5] Poirier P, Eckel RH. Obesity and cardiovascular disease. Curr Atheroscler Rep 2002;4:448–53.
[6] Matsuzawa Y. Therapy Insight: adipocytokines in metabolic syndrome and related cardiovascular disease. Nat Clin Pract Cardiovasc Med 2006;3:35–42.
[7] Fujioka S, Matsuzawa Y, Tokunaga K, Tarui S. Contribution of intra-abdominal fat accumulation to the impairment of glucose and lipid metabolism in human obesity. Metabolism 1987;36:54–9.
[8] Nakamura T, Tokunaga K, Shimomura I, et al. Contribution of visceral fat accumulation to the development of coronary artery disease in non-obese men. Atherosclerosis 1994;107:239–46.
[9] Yamamoto M, Egusa G, Hara H, Yamakido M. Association of intraabdominal fat and carotid atherosclerosis in non-obese middle-aged men with normal glucose tolerance. Int J Obes Relat Metab Disord 1997;21:948–51.
[10] Kim SK, Kim HJ, Hur KY, et al. Visceral fat thickness measured by ultrasonography can estimate not only visceral obesity but also risks of cardiovascular and metabolic diseases. Am J Clin Nutr 2004;79:593–9.
[11] Liu KH, Chan YL, Chan JC, Chan WB. Association of carotid intima-media thickness with mesenteric, preperitoneal and subcutaneous fat thickness. Atherosclerosis 2005;179:299–304.
[12] Lear SA, Humphries KH, Kohli S, Frohlich JJ, Birmingham CL, Mancini GB. Visceral adipose tissue, a potential risk factor for carotid atherosclerosis: results of the Multicultural Community Health Assessment Trial (M-CHAT). Stroke 2007;38:2422–9.
[13] Kawamoto R, Ohtsuka N, Ninomiya D, Nakamura S. Association of obesity and visceral fat distribution with intima-media thickness of carotid arteries in middle-aged and older persons. Intern Med 2008;47:143–9.
[14] Snell-Bergeon JK, Hokanson JE, Kinney GL, et al. Measurement of abdominal fat by CT compared to waist circumference and BMI in explaining the presence of coronary calcium. Int J Obes Relat Metab Disord 2004;28:1594–9.
[15] Sutton-Tyrrell K, Newman A, Simonsick EM, et al. Aortic stiffness is associated with visceral adiposity in older adults enrolled in the study of health, aging, and body composition. Hypertension 2001;38:429–33.
[16] Orr JS, Gentile CL, Davy BM, Davy KP. Large artery stiffening with weight gain in humans: role of visceral fat accumulation. Hypertension 2008;51:1519–24.
[17] Kanai H, Hasegawa H, Ichiki M, Tezuka F, Koiwa Y. Elasticity imaging of atheroma with transcutaneous ultrasound: preliminary study. Circulation 2003;107:3018–21.
[18] Hasegawa H, Kanai H, Hoshimiya N, Koiwa Y. Evaluating the regional elastic modules of a cylindeicl shell with nonuniform wall thickness. J Med Ultrason 2004;31:81–90.
[19] Kanai H, Sato M, Koiwa Y, Chubachi N. Transcutaneous measurement and spectrum analysis of heart wall vibrations. IEEE Trans Ultrason Ferroelectr Freq Control 1996;43:791–810.
[20] Kanai H, Koiwa Y, Zhang J. Real-time measurement of local myocardium motion and arterial wall thickening. IEEE Trans Ultrason Ferroelectr Freq Control 1999;46:1229–41.
[21] Okimoto H, Ishigaki Y, Koiwa Y, et al. A novel method for evaluating human carotid artery elasticity: possible detection of early stage atherosclerosis in subjects with type 2 diabetes. Atherosclerosis 2008;196:391–7.
[22] Hasegawa H, Kanai H, Hoshimiya N, Chubachi N, Koiwa Y. Accuracy evaluation in the measurement of a small change in the thickness of arterial walls and the measurement of elasticity of the human carotid artery. Jpn J Appl Phys 1998;37:3101–5.
[23] Sidhu PS, Desai SR. A simple and reproducible method for assessing intimal–medial thickness of the common carotid artery. Br J Radiol 1997;70:85–9.
[24] Munakata M, Ito N, Nunokawa T, Yoshinaga K. Utility of automated brachial ankle pulse wave velocity measurements in hypertensive patients. Am J Hypertens 2003;16:653–7.
[25] Kvist H, Sjostrom L, Tylen U. Adipose tissue volume determinations in women by computed tomography: technical considerations. Int J Obes 1986;10:53–67.
[26] Bjorntorp P. Metabolic implications of body fat distribution. Diabetes Care 1991;14:1132–43.
[27] Takami R, Takeda N, Hayashi M, et al. Body fatness and fat distribution as predictors of metabolic abnormalities and early carotid atherosclerosis. Diabetes Care 2001;24:1248–52.
[28] Ingelsson E, Sullivan LM, Fox CS, et al. Burden and prognostic importance of subclinical cardiovascular disease in overweight and obese individuals. Circulation 2007;116:375–84.
[29] Yamada J, Tomiyama H, Matsumoto C, et al. Overweight body mass index classification modifies arterial stiffening associated with weight gain in healthy middle-aged Japanese men. Hypertens Res 2008;31:1087–92.
[30] Kvist H, Chowdhury B, Sjostrom L, Tylen U, Cederblad A. Adipose tissue volume determination in males by computed tomography and 40K. Int J Obes 1988;12:249–66.

BRAIN RESEARCH 1263 (2009) 58–68

available at www.sciencedirect.com

ScienceDirect

www.elsevier.com/locate/brainres

BRAIN RESEARCH

Research Report

Obesity alters circadian expressions of molecular clock genes in the brainstem

Keizo Kaneko[a,b,1], Tetsuya Yamada[a,1], Sohei Tsukita[a,b], Kei Takahashi[a,b], Yasushi Ishigaki[a], Yoshitomo Oka[a,2], Hideki Katagiri[b,*,2]

[a]Division of Molecular Metabolism and Diabetes, Tohoku University Graduate School of Medicine, 2-1 Seiryo-machi, Aoba-ku, Sendai 980-8575, Japan

[b]Division of Advanced Therapeutics for Metabolic Diseases, Center for Translational and Advanced Animal Research, Tohoku University Graduate School of Medicine, 2-1 Seiryo-machi, Aoba-ku, Sendai 980-8575, Japan

ARTICLE INFO

Article history:
Accepted 30 December 2008
Available online 15 January 2009

Keywords:
Obesity
Insulin resistance
Circadian rhythm
Clock gene
Nucleus of the solitary tract
Metabolic syndrome

ABSTRACT

Major components of energy homeostasis, including feeding behavior and glucose and lipid metabolism, are subject to circadian rhythms. Recent studies have suggested that dysfunctions of molecular clock genes are involved in the development of obesity and diabetes. To examine whether metabolic states per se alter the circadian clock in the central nervous system (CNS), we analyzed the daily mRNA expression profiles of core clock genes in the caudal brainstem nucleus of the solitary tract (NTS). In lean C57BL/6 mice, transcript levels of the core clock genes (*Npas2*, *Bmal1*, *Per1*, *Per2* and *Rev-erbα*) clearly showed 24-h rhythmicity. On the other hand, the expression profiles of *Bmal1* and *Rev-erbα* were attenuated in mice with high fat diet-induced obesity as well as genetically obese KK-A^y and *ob/ob* mice. *Clock* expression levels were increased in mice with high fat diet-induced obesity and *Cry1* expression levels were decreased in KK-A^y and *ob/ob* mice. In addition, peroxisome proliferator-activated receptor α (PPARα), which reportedly increases the BMAL1 transcriptional level, was up-regulated in the NTS of these murine models of obesity and insulin resistance, suggesting involvement of PPARα in the attenuation of circadian rhythms in the NTS in obese states. Furthermore, a circadian expression profile of a downstream target of clock genes, the large conductance Ca^{2+}-activated K^+channel, was disturbed in the NTS of these murine obesity models. These perturbations might contribute to neuronal dysfunction in obese states. This is the first report showing that obesity perturbs the circadian expressions of core clock genes in the CNS.

1. Introduction

The worldwide prevalence of obesity and type 2 diabetes mellitus (T2DM) is increasing at an alarming rate, with major adverse consequences for human health (Flier, 2004). Since body weight and adiposity are maintained within a narrow range under steady state environmental conditions, the concept that a homeostatic center for energy metabolism

* *Corresponding author.* Fax: +81 22 717 8228.
E-mail address: katagiri@mail.tains.tohoku.ac.jp (H. Katagiri).
[1] Contributed equally.
[2] Contributed equally.

0006-8993/$ – see front matter © 2009 Published by Elsevier B.V.
doi:10.1016/j.brainres.2008.12.071

exists has been widely accepted and there is a growing consensus that this regulatory center is located mainly in the central nervous system (CNS), especially in the hypothalamus (Sandoval et al., 2008). Humoral factors, including insulin and adipokines, and afferent nerve signals (Uno et al., 2006); (Yamada et al., 2006) are known to be very important for conveying information regarding peripheral energy status to the CNS (Katagiri et al., 2007); (Yamada et al., 2008). We have proposed that the brain integrates and processes the peripheral metabolic information to send signals that control systemic metabolism (Katagiri et al., 2007).

Major components of energy homeostasis, such as feeding behavior and glucose and lipid metabolism, are subject to circadian rhythms. These rhythms are regulated by a circadian clock system composed of transcriptional/translational feedback loops that are now recognized to cycle in the suprachiasmatic nucleus (SCN) of the hypothalamus as well as in most peripheral tissues (Ramsey et al., 2007). In brief, each cell contains a set of core clock genes – *Clock*, *Bmal1*, *Cry* 1-2, *Per* 1-3 and nuclear receptors (*Rev-erbα*, *ROR*). The CLOCK/BMAL1 heterodimer regulates the production of proteins such as PER and CRY, which in turn regulate the production of BMAL1 (Schibler and Sassone-Corsi, 2002). Through these feedback loops, core clock gene expressions generate an endogenous rhythm of numerous protein expressions, leading to rhythmic functioning of cells and tissues that oscillates over an approximately 24-hour period (Dunlap, 2006). The molecular clock has been demonstrated to modulate energy metabolism by controlling the expression and activity of numerous enzymes, transport systems and nuclear receptors involved in lipid and carbohydrate metabolism (Ramsey et al., 2007); (Staels, 2006); (Yang et al., 2006).

Recent studies have suggested that, in murine models, malfunctioning of molecular clock genes, such as *Bmal1* (Rudic et al., 2004) and *Clock* (Turek et al., 2005), is involved in development of the metabolic syndrome. In addition, in humans, prevalences of obesity, T2DM and features of the metabolic syndrome are reportedly increased in nightshift workers and men with short sleep durations (Prasai et al., 2008). Thus, the importance of the molecular clock for many metabolic processes has been extensively documented. On the other hand, to our knowledge, there have been no studies showing that obesity itself attenuates rhythmic expressions of clock genes in the CNS. Rather, a high fat diet does not affect rhythmic expression profiles of core clock genes, such as *Bmal1* and *Per2*, in the mediobasal hypothalamus, whereas it does attenuate circadian expression of these core clock genes in the liver and adipose tissue (Kohsaka et al., 2007). In genetically obese and diabetic mice as well, circadian expression of neither *Per1* nor *Per2* is altered in the suprachiasmatic nucleus (SCN), while both are attenuated in the liver (Kudo et al., 2004). Based on these findings, the idea that obesity affects molecular clock function in peripheral tissues but not centrally has been proposed (Prasai et al., 2008). However, metabolic alterations disturb the patterns and/or circadian rhythmicity of behaviors, such as sleep-wake cycle (Danguir, 1989); (Jenkins et al., 2006); (Laposky et al., 2006); (Megirian et al., 1998), locomotor activity and feeding (Kohsaka et al., 2007), indicating rhythmic perturbation in the CNS. Therefore, in the present study, we examined whether obesity per se alters circadian expressions of clock genes in the CNS, especially in the caudal brainstem nucleus of the solitary tract (NTS).

Recently, we have demonstrated that alterations in fat accumulation in intra-abdominal organs, such as visceral adipose tissue and the liver, send afferent neuronal signals to the brain, leading to modulation of feeding behavior as well as efferent sympathetic tonus (Uno et al., 2006); (Yamada et al., 2006). These neuronal signals are likely to initially be processed mainly by the NTS (Grill, 2006); (Schwartz, 2006), since the NTS receives neuronal projections of vagal and non-vagal afferents (Menetrey and Basbaum, 1987); (Menetrey and De Pommery, 1991). In addition, humoral factors, such as leptin, insulin and glucose, may directly impinge on neuronal activities in the NTS (Grill, 2006); (Schwartz, 2006). Furthermore, the NTS and the hypothalamic nuclei send neuronal projections to each other. Thus, we postulate that the NTS is ideally situated for integrating central and peripheral metabolic signals. Therefore, we focused on the circadian expressions of clock genes in the NTS.

2. Results

2.1. *Rhythmic mRNA expressions of clock genes in the NTS of C57BL/6 mice*

To investigate whether the mRNA expressions of clock genes show circadian rhythms in the NTS, we first analyzed wild-type lean control mice, 10-week-old C57BL/6 mice fed a regular chow diet (CD mice). Bilateral NTS samples at the level of the area postrema were obtained every 4 h throughout a single 24-h period employing a laser micro-dissection procedure (Fig.1A). *Clock* and *Cry1* expressions did not show circadian rhythms in the NTS (Fig. 1B). In contrast, other clock genes we examined (*Npas2* (a *Clock* homolog), *Bmal1*, *Per1*, *Per2* and *Rev-erbα*) all exhibited 24-h rhythmicity. The transcript levels of *Bmal1* and *Npas2* peaked in the first half of the light phase. On the other hand, the *Per1* and *Per2* mRNA simultaneously dropped to near trough levels (Fig. 1B). The NPAS2/BMAL1 complex reportedly induces transcription of *Per* genes (Reick et al., 2001). In addition, the rhythmicity of these clock genes was also observed in the NTS of 15-week-old C57BL/6 mice and no significant differences in the expression profiles of these clock genes were detected between 10-and 15-week-old C57BL/6 mice (Fig. 1C). These results indicate that an intracellular circadian clock system actually operates in the NTS.

2.2. *Alterations in circadian mRNA expression profiles of clock genes in the NTS of obesity models*

Next, we examined whether obesity affects the circadian expressions of clock genes in the NTS. As shown in Fig. 2, C57BL/6 mice fed a high fat diet for 10 weeks (HFD mice), KK-A^y and *ob/ob* (leptin-deficient) mice were significantly heavier than CD mice. Serum insulin levels were significantly increased in all these murine obesity models. In addition, blood glucose levels were markedly increased in KK-A^y and *ob/ob* mice. Serum leptin levels were also increased in HFD and KK-A^y mice. Serum free fatty acid levels were markedly increased in KK-A^y and *ob/ob* mice but

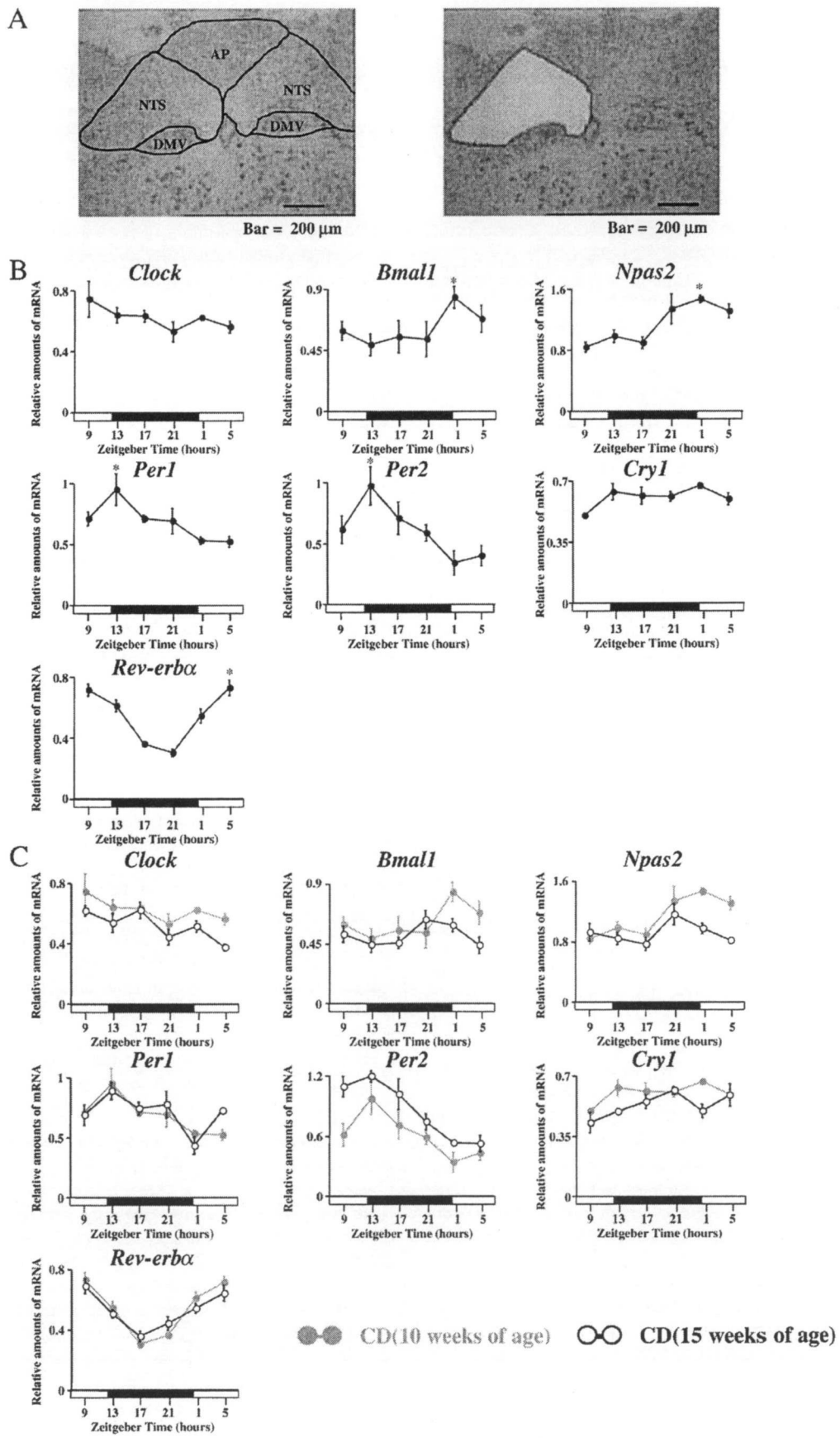
A
AP
NTS
NTS
DMV
DMV
Bar = 200 μm
Bar = 200 μm
B
Clock
Bmal1
Npas2
Per1
Per2
Cry1
Rev-erbα
Relative amounts of mRNA
Zeitgeber Time (hours)
C
Clock
Bmal1
Npas2
Per1
Per2
Cry1
Rev-erbα
CD(10 weeks of age)
CD(15 weeks of age)

not in HFD mice (Fig. 2). These findings suggest that severe insulin resistance is induced in KK-A^y and *ob/ob* mice, while that in HFD mice is milder.

To examine the hypothesis that obesity affects expressions of clock genes, we analyzed the circadian expressions of transcripts encoding CLOCK, NPAS2, BMAL1, PER1, PER2, CRY1 and REV-ERBα in the NTS of these murine obesity models. The rhythms and levels of expressions of these clock genes in the NTS of murine obesity models were compared with those in age-matched CD mice (HFD mice vs 15-week-old CD mice and KK-A^y and *ob/ob* mice vs 10-week-old CD mice). As shown in Fig. 3, the levels of *Clock* expression were significantly increased at several observation times in HFD mice. Interestingly, rhythms of *Bmal1* expression in the NTS were significantly altered in HFD (2-way ANOVA; $F=11.54$, $P=2.0\times10^{-7}$) and KK-A^y (2-way ANOVA; $F=4.01$, $P=4.9\times10^{-3}$) mice and levels were significantly increased in HFD, KK-A^y and *ob/ob* mice. The *Per2* expression level tended to be increased in KK-A^y mice, although the difference did not reach statistical significance. The *Cry1* expression level was significantly decreased in KK-A^y and *ob/ob* mice. Furthermore, in addition to decreased expression levels of *Rev-erbα*, the rhythms of its expression were significantly altered in the NTS of HFD (2-way ANOVA; $F=2.49$, $P=4.6\times10^{-2}$), KK-A^y (2-way ANOVA; $F=12.02$, $P=3.0\times10^{-7}$) and *ob/ob* mice (2-way ANOVA; $F=7.90$, $P=2.8\times10^{-5}$) (Fig. 3). Collectively, these findings suggest that obesity with insulin resistance alters profiles of rhythmic clock gene expressions in the NTS and generates gene-specific changes in circadian expression patterns.

2.3. *The mRNA expression profiles of clock-related genes in the NTS of obesity models*

What mechanisms alter the expression profiles of clock genes? Transcriptional activity of peroxisome proliferator-activated receptor α (PPARα), a member of the nuclear receptor superfamily, is up-regulated in the livers of mice with obesity and diabetes (Memon et al., 2000). In addition, the CLOCK/BMAL1 heterodimer activates the transcription of PPARα, which then binds to the peroxisome proliferator response element and thereby induces *Bmal1* transcription in the liver (Canaple et al., 2006). In addition, PPARα is reportedly expressed in the NTS, but not in the hypothalamus (Moreno et al., 2004). These findings prompted us to theorize that PPARα affects the mRNA expression profiles of clock genes. Therefore, we analyzed mRNA expression profiles of PPARα in the NTS of CD mice as well as that of murine models of obesity and insulin resistance. In both CD and obese mice (HFD, KK-A^y and *ob/ob* mice), PPARα expression in the NTS showed no 24-h rhythmicity (Fig. 4A). However, the mRNA expression level of PPARα was significantly increased in the NTS of HFD and KK-A^y mice. In addition, in the NTS of *ob/ob* mice, the PPARα expression level tended to be increased and *carnitine palmitoyltransferase-1α* (CPT1α), a downstream target of PPARα, was significantly up-regulated, suggesting functional activation of PPARα (Fig. 4A). Thus, PPARα in the NTS might be involved in the altered expression profiles of clock genes.

Next, to investigate whether alterations in circadian expressions of clock genes affect neuronal function in the NTS, we analyzed the mRNA expression levels of downstream targets of clock genes, *Kcnma1* and *tyrosine hydroxylase* (*TH*), both of which are involved in neuronal activity. Daily expression of *Kcnma1*, the large conductance Ca^{2+}-activated K^+(BK) channel, is reportedly controlled by the intrinsic circadian clock in the SCN (Meredith et al., 2006); (Panda et al., 2002). The circadian expression profile of *TH*, the rate-limiting enzyme in catecholamine synthesis, is also affected by *Clock* in the midbrain ventral tegmental area (McClung et al., 2005). As reportedly observed in the SCN (Panda et al., 2002), *Kcnma1* in the NTS of CD mice was highly expressed in the early portion of the dark phase (Fig. 4B). In contrast, this *Kcnma1* expression pattern disappeared and expression levels were markedly decreased in the NTS of all three murine obesity models (Fig. 4B). In addition, *TH* expression levels in *ob/ob* mice were significantly decreased as compared to those in CD mice (Fig. 4B). Collectively, obesity-induced alterations in expression profiles of clock-related genes, such as *Kcnma1* and *TH*, might elicit neuronal dysfunctions in the NTS, although further studies are needed to confirm this possibility.

3. Discussion

In the present study, we demonstrated the circadian expressions of a series of core clock genes in the NTS of lean wild-type mice. In addition, the circadian expressions of core clock genes and their downstream targets were shown to be attenuated in the NTS of obesity models, suggesting the involvement of NTS rhythmic perturbation in further metabolic deterioration in the obese state.

Metabolism is coordinated and regulated among different organs/tissues throughout the body. This coordinated metabolic regulation is apparently essential for maintaining systemic homeostasis, particularly energy metabolism. Metabolic communication among organs/tissues and integration of metabolic information in various tissues thus appears to be important and perturbation of this control system may lead to the development of metabolic disorders (Katagiri et al., 2007). This controlling system is likely to consist of afferent and efferent limbs as well as a central control mechanism putatively situated in the CNS (Yamada et al., 2008). For the afferent limb, there are two avenues, humoral factors and

Fig. 1 – Rhythmic mRNA expressions of clock genes in the NTS of C57BL/6 mice. (A) Coronal section of mouse brainstem within the NTS region of before laser micro-dissection (left). The NTS removed at the area postrema level (right). AP, area postrema; DMV, dorsal motor nucleus of the vagus. (B) Daily mRNA expression profiles of *clock* genes in the NTS of 10-week-old C57BL/6 mice, which had been maintained under a 12-h light, 12-h dark cycle and fed a standard diet. (C) Daily mRNA expression profiles of *clock* genes in the NTS of 15-week-old C57BL/6 mice (○-○), which had been maintained under a 12-h light, 12-h dark cycle and fed a standard diet. Data are presented as means ± SE ($n=4$–5/group). 1-way ANOVA demonstrates significant rhythmicity of *Npas2*, *Bmal1*, *Per1*, *Per2* and *Rev-erbα* mRNA levels ($P<0.05$). *Indicates peaks of rhythmically expressed each mRNA.

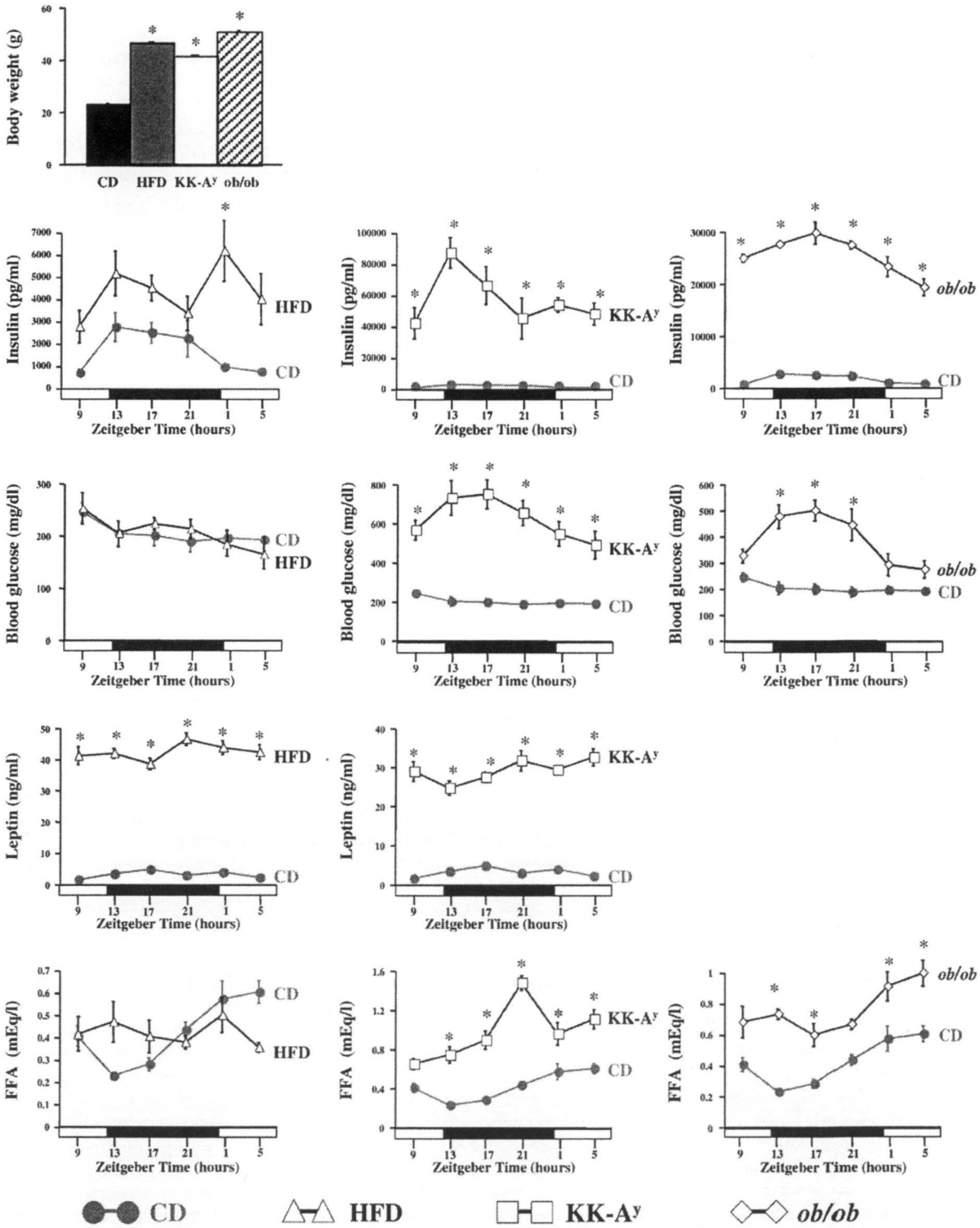

Fig. 2 – Metabolic parameters of murine obesity models. Body weight and diurnal variations in blood glucose, serum insulin, leptin and free fatty acid (FFA) levels of CD mice (●–●), HFD mice (△–△), KK-A^y mice (□–□) and *ob/ob* mice (◇–◇). Data are presented as means ± SE (n=4–5/group). Body weights were analyzed by 1-way ANOVA. The statistical significance of differences between two groups was determined using 2-way ANOVA followed by Tukey's post hoc test. *Indicates $P<0.05$.

afferent neuronal signals. For instance, mechanical, nutrient chemical and gut peptide signals are sent from the gastrointestinal tract by primary afferent neurons of the vagus and from the dorsal root (Badman and Flier, 2005). In addition, we have recently demonstrated that information regarding lipid metabolism in intra-abdominal tissues, such as visceral adipose tissue and the liver, is conveyed to the brain via afferent nerves, leading to modulation of feeding behavior and sympathetic tonus (Uno et al., 2006); (Yamada et al., 2006). These neuronal signals are initially processed mainly by the NTS (Grill, 2006); (Schwartz, 2006). In addition, receptors for humoral factors, such as leptin and insulin, are reportedly expressed on NTS neurons (Grill, 2006); (Schwartz, 2006). Furthermore, the NTS sends projections to other autonomic nuclei at all levels of the neuroaxis, including major targets in the hypothalamus, pons and medulla (Hermes et al., 2006). NTS neurons in turn receive descending projections from a variety of hypothalamic nuclei implicated in the control of energy homeostasis (Grill, 2006); (Schwartz, 2006). Thus, the NTS seems to be ideally situated to integrate central and peripheral signals. In the present study, the circadian expressions of a series of core clock genes, including *Npas2*, *Bmal1*, *Per1*, *Per2* and *Rev-erbα*, were demonstrated in the NTS of lean wild-type mice, results consistent with those of a previous report describing rhythmic expressions of *Bmal1* and *Per2* in the rat NTS (Herichova et al., 2007).

Recent studies have suggested that rhythmic abnormalities affect energy homeostasis as well as glucose and lipid metabolism (Prasai et al., 2008); (Rudic et al., 2004); (Turek et al., 2005). Metabolic perturbation, in turn, reportedly induces dysregulation of circadian rhythms in the periphery. In fact, both genetically induced and high fat diet-induced obesity attenuates the circadian expressions of a number of clock genes in peripheral tissues, such as adipose and the liver (Ando et al., 2006); (Ando et al., 2005); (Kohsaka et al., 2007); (Kudo et al., 2004). In addition, metabolic alterations disturb patterns and/or the circadian rhythmicity of behaviors, such as the sleep-wake cycle, locomotor activity and feeding. For example, mice fed a high-fat diet have longer sleep times but less sleep consolidation (Jenkins et al., 2006). Genetic mouse (Laposky et al., 2006) and rat (Danguir, 1989); (Megirian et al., 1998) models of obesity exhibit disrupted sleep-wake patterns. High-fat diet also leads to changes in the period of locomotor activity and feeding rhythm in mice (Kohsaka et al., 2007). Since these behavioral abnormalities indicate CNS dysfunction, these findings suggest circadian malfunction in the CNS. However, obesity reportedly has no effects molecular clock genes in the hypothalamus (Kohsaka et al., 2007) and the SCN (Kudo et al., 2004). In the present study, we showed both high fat diet-induced and genetically induced obesity to affect circadian expression profiles of core clock genes, such as *Clock*, *Bmal1*, *Rev-erbα* and *Cry1* in the NTS. This is the first report to demonstrate that circadian expression profiles of clock genes in the CNS are perturbed by obesity.

A major question arising from these findings involves the nature of the molecular link between the regulation of metabolism and the circadian rhythmicity of clock genes. We showed that both PPARα transcription and the *Bmal1* expression level were increased in the NTS of obese mice. Obesity reportedly enhances PPARα transcriptional activity in the liver (Memon et al., 2000). PPARα binds to the PPRE and induces transcription of *Bmal1* (Canaple et al., 2006). In addition, amplitudes of *Bmal1* expression are reportedly decreased in the livers of PPARα knockout mice (Canaple et al., 2006), which is in line with the findings of this study. Therefore, PPARα might be directly involved in obesity-induced enhancement of *Bmal1* expression in the NTS, although further studies are needed to confirm this conclusion. Furthermore, we found that *Rev-erbα* expression was decreased in the NTS of obese mice. *Rev-erbα* transcription is inhibited by retinoic acid (Chawla and Lazar, 1993), levels of which are increased in the metabolic syndrome (Yang et al., 2005). These findings prompt us to hypothesize that high concentrations of retinoic acid would decrease expression levels of *Rev-erbα* in the NTS of mice with obesity and insulin resistance. In addition, because *Bmal1* transcription is inhibited by REV-ERBα (Chawla and Lazar, 1993); (Preitner et al., 2002), decreased *Rev-erbα* expression may in turn contribute to increased *Bmal1* expression.

Finally, we showed that the expression profiles of downstream targets of clock genes were affected by obesity associated with insulin resistance. The expression profile of *Kcnma1*, a downstream target of clock genes (Meredith et al., 2006); (Panda et al., 2002), was attenuated in the NTS of obese mice. Since the BK channel is believed to play a critical role in the control of neurosecretion (Lara et al., 1999); (Lovell and McCobb, 2001), attenuated expression of *Kcnma1* might underlie the neuronal dysfunction in obese states. In addition, *TH* mRNA expression was decreased in the NTS of *ob/ob* mice. Recent reports have demonstrated that neural pathways from catecholamine neurons in the NTS to the hypothalamus are involved in energy homeostasis (Date et al., 2006); (Ritter et al., 2003). Therefore, these findings suggest that perturbation of circadian expression profiles of clock genes in the NTS is involved in further metabolic deterioration of energy homeostasis.

In summary, this study showed that a series of core clock genes exhibit circadian rhythms in the NTS of the brainstem. However, these rhythmic expressions are perturbed in murine models with high fat diet-induced or genetically induced obesity and insulin resistance. Obesity also alters expressions of PPARα and downstream targets of clock genes, which might account for the mechanisms underlying the rhythmic disruption and neuronal dysfunction in obese states. This is the first report showing that obesity perturbs the circadian expressions of core clock genes in the CNS.

4. Experimental procedures

4.1. Animals

Male C57BL/6 mice (Kyudo, Kumamoto, Japan), KK-A^y mice (CLEA Japan, Tokyo, Japan) and *ob/ob* mice (strain C57BL/6 *ob/ob*) (Charles River Japan, Yokohama, Japan) were obtained and maintained under specific-pathogen free conditions with controlled temperature and humidity and a 12-h light (0600–1800), 12-h dark (1800–0600) cycle. According to the breeder

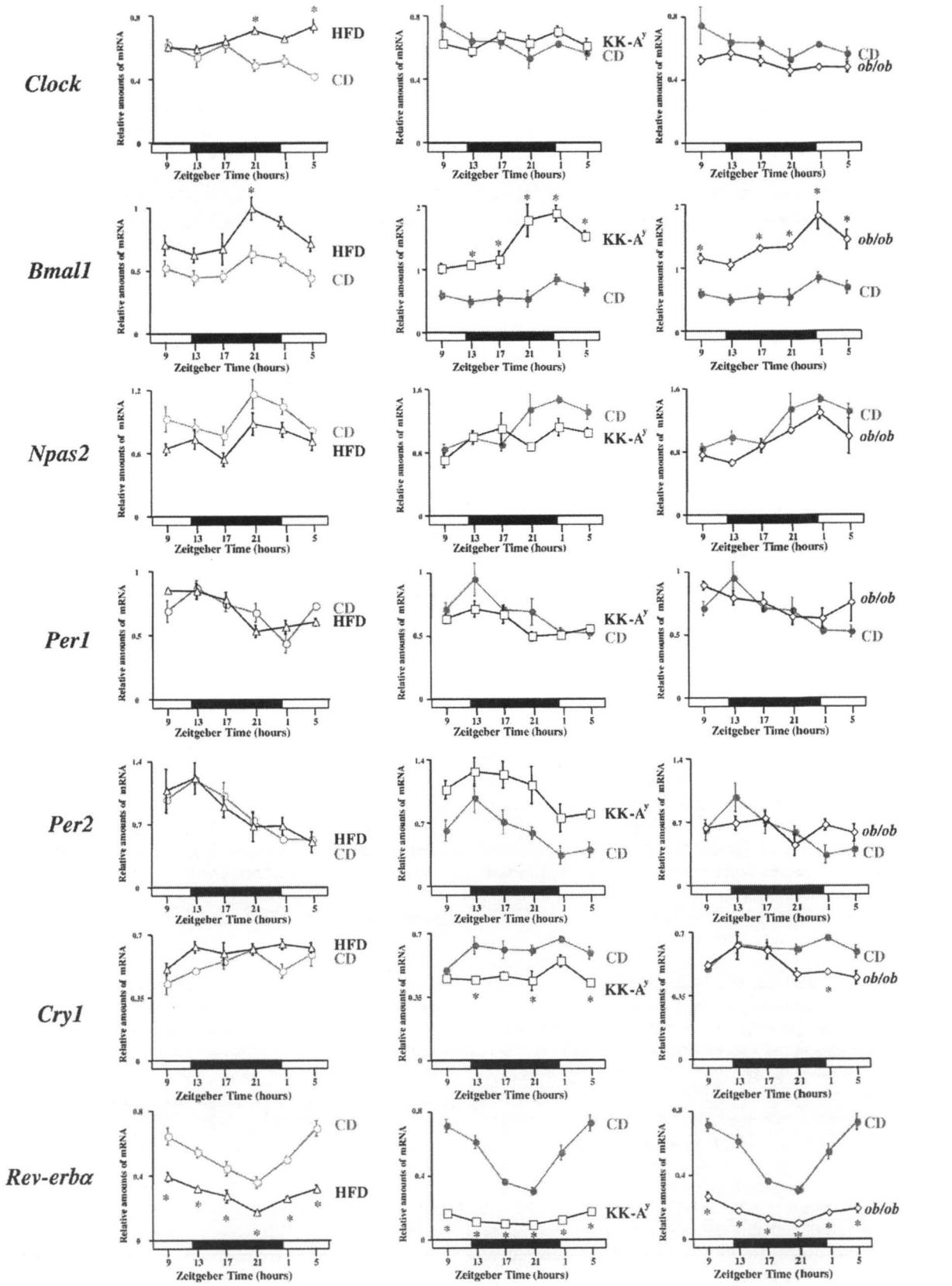
Clock
Bmal1
Npas2
Per1
Per2
Cry1
Rev-erbα
Relative amounts of mRNA
Zeitgeber Time (hours)
HFD
CD
KK-A^y
ob/ob
CD(10 weeks of age)
CD(15 weeks of age)